Photogrammetric Techniques for Evaluation and Analysis of Concrete Structures and Specimens

By

Nicolas D'Amico

Bachelor of Science in Civil and Environmental Engineering

University of Massachusetts Lowell (2017)

Submitted to the Department of Civil and Environmental Engineering

in partial fullfillment of the requirements for the degree of

Master of Science in Structural Engineering

UNIVERSITY OF MASSACHUSETTS LOWELL

(May) 2017

Author .....

Department of Civil and Environmental Engineering

April 21, 2017

Thesis Supervisor .....

Professor Tzuyang Yu

Department of Civil and Environmental Engineering

Commitee Member .....

Professor Donald Leitch

Department of Civil and Environmental Engineering

Commitee Member .....

Professor Susan Farajii

Department of Civil and Environmental Engineering

Photogrammetric Techniques for Evaluation and Analysis of Concrete Structures and Specimens

by

Nicolas D'Amico

Submitted to the Department of Civil and Environmental Engineering
on April 21, 2017, in partial fulfillment of the
requirements for the degree of
Masters of Science in Civil and Environmental Engineering

Abstract

Photogrammetric methods such as structure from motion (SFM) have the capabilities to produce models with accurate geometric, surface and mechanical informationby generating point cloud models (PCM). PCM can be used for visual inspection and data registration in condition assessment. Laboratory concrete specimens and in-situ reinforced concrete structures (e.g., buildings and bridges) were constructed and evaluated for demonstrating the practical usage and geometric accuracy of PSM. Results show that photogrammetric methods can be used for remote sensing and nondestructive testing (NDT) in maintaining againg civil infrastructure. From this research, it is found that photgrammetric methods are capable pf delivering PCM with geometric accuracy less than 5% error in surface crack profiling, damage assessment, area and volume estimation, and data registration. Estimated mechanical properties from PCM can also be correlated and used in finite element analysis for condition assessment.

Thesis Supervisor: Tzuyang Yu
Title: Associate Professor

Acknowledgments

While it is not possible to thank all of the people in my life who've helped to shape me as an individual I would like to thank the following significant people for their influence in my life.

First, Professor Tzuyang Yu, who always pushed me towards success. Thank you for being a consistent mentor, advisor, teacher, and friend. There is no scale on which I could explain to you the tremendous effect you have had on my life and of course my research.

To my family, all of you helped to shape me from the time we were children into the person I am today. A person with the right focus, passion, and confidence to complete this masters Thesis. I love you all very much, words can not explain the gratitude I feel toward all of my siblings, and to my parents for pushing me, believing in me, and for being there when I needed you.

Contents

List of Figures

List of Tables

Chapter 1

Introduction

Civil engineers have the exclusive responsibility to maintain the safety of civil infrastructure by inspecting and monitoring existing and aged infrastructure systems. It is of utmost importance that researchers pursue and develop effective and efficient non-destructive evaluation/testing/inspection (NDE/T/I) techniques. To be effective, the techniques must be easy to use as well as accurate. To be efficient the techniques must be inexpensive and fast in data collection. Current federal and state standards for inspection rely heavily on visual inspection by professional engineers. These techniques are not only subjective, but have non–quantifiable parameters and therefore are not a sufficient long term solution to the problems associated with a severely deteriorating infrastructure as we see now in the United States. NDE currently in practice or being researched includes, visual techniques such as photogrammetric analysis, light detection and ranging (LiDAR), and laser imaging. As well as acoustic rebound hammer, Synthetic aperture radar (SAR) imaging, ground penetrating radar (GPR), thermal imaging, and many other techniques. Additionally, the expansion of the market for unmanned aerial vehicles (UAV) adds a feasibility to many NDE research fields as UAV allow for a more versatile approach to many accessibility problems. UAV allow engineers to collect data from hard-to-reach places without being put into harms way.

In this Thesis, the NDE technique primarily considered is photogrammetric structure from motion (SFM) point cloud modeling (PCM) using terrestrial, as well as airborne platforms for data acquisition. This method was chosen due to its efficiency

and effectiveness.

1.1 Research objective

The contribution of this research is to investigate how photogrammetry can be used to create geometrically accurate point cloud models which can be used on laboratory specimen as well as in-situ structures. Furthermore how PCM can be used for visual inspection as well as data integration of Synthetic aperture radar (SAR), rebound hammer (RBH) and digital image correlation results(DIC). As well as how photogrammetric PCM can be used to conduct condition assessment including geometric analysis, surface crack profiling, mechanical loading analysis and even finite element modeling (FEM).

1.2 Thesis approach

This study presents an approach to collect, organize, calibrate and effectively evaluate PCM for geometrically accurate visual inspection, data registration, and condition assessment of concrete structures and specimen. It is the desire of the research to, conceptualize, prove the feasibility, and provide a framework for researchers and engineers to use to produce meaningful results.

1.3 Organization of thesis

The organization of the thesis is illustrated in the following **Chapter 2** consists of literature review on photogrammetric techniques, as well as UAV technologies. **Chapter 3** Introduces the methodology, and framework of and for analyzing accuracy of PCM, for evaluating laboratory specimens as well in-situ structures for civil infrastructure maintenance. **Chapter 4** provides a compilation of the results collected with respect to laboratory specimens for the accuracy analysis and condition assessment of concrete specimens. **Chapter 5** provides a compilation of the results

collected on in-situ structures, and their interpretation for inspection, data registration, and condition assessment of civil structures. **Chapter 6** Summarizes the research findings and major contributions. Suggested future research is additionally outlined. **Appendices A and B** Detail additional tables and figures, respectively.

Chapter 2

Literature Review

2.1 Overview of photogrammetry

Photogrammetric techniques employ the capabilities of photoscanning algorithms which calculate fiducial key points to effectively calculate the disparities within the triangulations of two dimensional (2D) photographs in order to construct a three dimensional (3D) point cloud models(PCM)[15]. These techniques have been used for a wide range of problems. From architectural remediation and conservation, video-game design, surveying, geological modeling and many more. PCM can be constructed from light detection and ranging (LiDAR) system, terrestrial laser scanner(TLS), or photogrammetric data. PCM will be further explained in a later section but a brief introduction is given here for reader continuity. PCM can be thought of as a geometric reconstruction of any 3D object based on thousands, or even millions of points. A TLS or LiDAR system directly scans a target and plots the distances in space from an initial setup. Photogrammetry on the other hand, uses triangulation algorithms to calculate the relative distances and plot them in space. Both TLS, and photogrammetric techniques are valid for constructing PCM. Depending on the situation it is important to outweigh the benefits and sacrifices in the selection. TLS lacks accessibility, and is much more expensive,it also lacks photo-realism and generally requires extensive training. Photogrammetry requires only a camera to produce accurate photo-realistic models. Photogrammetry, however, is largely dependent on

the surveyors abilities, and is much more labor intensive. Ideal PCM would be constructed from integration of both techniques, but photogrammetric techniques are largely accessible and as such are the major discussion for this research.

Civil engineers most prominently use photogrammetric methods along with unmanned aircraft vehicle (UAV) technologies to survey land. By using a UAV to collect aerial photographs, a 3D terrain of a plot of land can be calculated.[5]. However, it is of growing belief that photogrammetry can serve to produce much more complicated and valuable information. In order to do so, photographic data must be used to construct large and geometrically accurate three dimensional (3D) objects in a computer aided world for evaluation. Some photogrammetric techniques currently employed are discussed in the following, and are outlined in Figure 2.1.

Digital image correlation (DIC), uses a pattern of fiducial markings to measure differences in strain over time. Essentially, 2D DIC is the matching of the same points between two images before and after deformation. [37] DIC requires a multitude of fiducial markers to be effective. While it has been employed to produce meaningful results, DIC still has a number of problems within it's practical application capabilities.[21]. By requiring a suitable surface pattern for this approach, a significant investment of time is involved. Some approaches suggest the use of a projected pattern, this however would cause many problems in conjunction with a UAV platform, and thereby severely limits its capabilities for future use.

Image mosaicking (IM) stitches multiple images together in order to create a larger image.[7]. In IM models, typically the mosaicked image or images are fit to a predetermined geometry of a structure. IM provides visual information, but loses data about spalling, cracks, surface profiling, and relies on a relatively objective approach to the inspection of a system.[12]

Digital photography has come now to the point where it can potentially start to replace traditional and more expensive surveying methods. Structure from motion (SFM) is a system that is able to simultaneously recover a 3D point cloud model and camera positions using only images. [30] SFM uses a set of images of a scene from multiple perspectives to calculate geometric disparities and plot the 3D structure

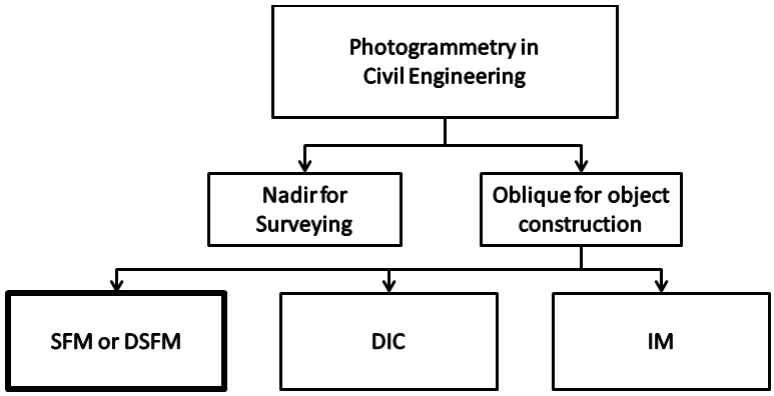

Figure 2-1: Photogrammetric platforms in civil engineering

in the form of a PCM [24]. For these reasons the close range(<10m) SFM oblique approach for object detection is used in this thesis. Accuracies in geometric determination of spacial data using this method have found to outperform total station data as well as laser scan point cloud data. SFM can produce PCM of high precision detail and accuracy, but it is subjugated to possible errors if the operator is not familiar with the sources of noise, error, and inconsistencies in the analysis of spacial point cloud information[28]. Close range photogrammetry is already used in civil, architectural, construction, and building management technologies. The ability to create complex 3D PCM provides complex illustrations for producing precise plans, preservation, virtual tours, time management, deformation calculations, even material testing[6]. Studies have shown the capabilities of photogrammetry to produce geometrically accurate information to a difference of 1 micrometer[23]. Yet accuracy in photogrammetry is strongly associated with distance from the perspective center, camera resolution and size of the object of interest. Unlike DIC methods SFM techniques do not require the use of additional fiducial markers in high quantities. Part of the reason for the success of SFM techniques in civil applications is concrete has a good natural texture which allows for keypoints to be automatically identified.[1]. Unlike plain, moving or very reflective surfaces, concrete provides perspective variance through its texture patterns. Several studies have verified the texture of concrete as sufficient for photogrammetry. Even in the difficult environments such as tunnels,

concrete and cast iron have proven sufficiently textured for (SFM) photogrammetric techniques [33].

However, photogrammetric techniques do not promise effective results. Due to the nature of optics, and computer analysis of the data, the question of reliability of accuracy becomes largely an issue of the photogrammetric surveyor's judgment. Errors in acquisition can cause noisy, and otherwise unrealistic portrayal of spacial data. even small calibration problems in a camera, or change in focal length can affect the outcome. Pivotal issues include but are not limited to, frame overlap, motion blurring perspective angle, poor resolution, or lack of sufficient data. The accuracy of the result also depends highly on the area cover by one pixel, i.e. the closer the data is acquired the higher accuracy the model is[13]. All low resolution, or unclear photographs should be removed before any processing is to be done. Raw image conversion to JPG format changes various settings affecting the quality of photogrammetric measurements. However, a comparison done by [25] showed nearly identical quality in models constructed from JPG compared to raw images. nonetheless, to ensure that no sacrifice in quality is being made, images in this thesis were kept in .PNG (loss-less format) when available. Airborn photgraphs were collected using the DJI phanton 3's buil in camera at 4k resolution. All terrestrial photographs were taken using a sixth generation Iphone, adding an additional parameter of multiple cameras. It was found that images can be collected with almost any digital camera without suffering from too many complications or limitations [4]. Therefore, this parameter was considered negligible in the construction of SFM PCM.

2.2 Point cloud models (PCM)

A PCM is a spacial representation of matrices of data in a 3D environment. From a modeling perspective, it is a cluster of known locations which can be used to construct a comprehensive 3D CAD or building information model (BIM) which indicates geometric information and can be used to integrate data of other formats. For construction companies this can mean effectively analyzing the work-flow of employees

and resources. For artists it means preserving the integrity of sculptors who are employed to construct concept art for virtual worlds[34]. For historians, geologists, and environmental scientists it means the detailed rendition of a structure or landmasses geometric and texture information. For civil engineers it is an effective surveying technique, but also can provide strain, crack detection, data integration, and general visual inspection capabilities.

When comparing terrestrial lasers to photogrammetric techniques, its imperative to understand that each has its own advantages and drawbacks. The accuracy of a TLS, PCM depends on the device precision. While a TLS suffers from high occlusion noise and lacks texture information, image-based 3D modeling depends on the accuracy of camera[35].

A combination of TLS or LiDAR methods is most appropriate for an exceedingly accurate PCM. A study conducted using both TLS and photogrammetric techniques to produce similar PCM showed that an integrated system with both TLS and photogrammetric methods will give more accurate results for 3D modeling documentation works. However, neither of the two methods was considered to be better than the other[19]. Each method produces very different outlier data, photogrammetry produces very obvious inconsistencies where the triangulation methods fail, warping the 3D environment to a best guess.

Lasers capture exactly what is in their scope, yet lack visual texture, and any additional information including even dust particles can sometimes be included. When using PCM removal of noise and additional information. is one of the most significant problems[26]. A combination technique would allow removal through PCM comparison, TLS precison and Photogrammetric realism.

PCM represent raw data in the form of thousands of points, upon first glance they can be very intimidating and hard to work with, the key is to manipulate the data using traditional modeling techniques as well as some that appeal to the uniqueness of this type of data.

This study used autodesks 123D catch, Agisoft photoscan, Meshlab, cloudcompare, and MatLab software packages to produce, analyze and manipulate the data

into intelligible information.

AutoDesk's 123D Catch and Agisofts Photoscan were used to process the photographs and to produce the results. These are photoscanning software packages which conduct the triangulation of many photographs into a 3D PCM. 123D Catch is a free, yet limited Autodesk software, whereas Agisoft's Photoscan is a commercial and much more powerful tool.

Meshlab, MatLab and Cloudcompare were used for the analysis, and manipulation of the data. Once in Meshlab, a local coordinate system can easily be manually defined. Transformation from relative to absolute coordinate systems is contingent on manual identification of global control points[38]. This means identifying a scale, and an understandable coordinate system. Scale can be added to a model simply by knowing the distance between two input points on a given model[4]. Cloudcompare, is used for the comparison of two point cloud models. In this study iterative closest point methods (ICP) were used to evaluate, and stitch point cloud information. ICP has been verified in literature for point cloud stitching using robotic kinematic information to estimate error on a relatively small surface in a laboratory setting[29]. It has also been used for mapping using a robotic 3D mapper [3], as well as in civil applications to stitch models together to test photogrammetric capabilities as a deflection, or strain guage measurement system[16].

2.3 Unmanned aircrafts as a photogrammetric tool

Photogrammetric modeling techniques require sufficient data from multiple perspectives to be effective. When assessing this consideration with regards to civil infrastructure the question of accessibility comes very quickly into play. With the introduction of UAV's into the market, modeling civil infrastructures obliquely much more possible as the "above-the-head" privileged point of view is the main motivation and key feature that makes photogrammetry and remote sensing much more feasible[9]. Furthermore, the advancements over the last decade in UAVs has rapidly enhanced image collection capabilities through improved stability and flight time of platforms, with

flight planning software now enabling survey design and optimized image capture[17]. The technological advancement of the UAV systems is burgeoning. from 2005 to 2013 number of times UAVs or UAS was referenced in research publications tripled [9]. The potential capabilities in terms of precision are only restricted by resolution of the image. Therefore, any level of precision could be reachable with the right type and number of ground control points [22]. Many of the useful applications in photogrammetry require the use of UAVs. Difficult to reach and unsafe areas are much more accessible with the inclusion of this technology. Crack detection in civil systems has been demonstrated to be effective reliable and feasible for full field mapping and health monitoring for civil infrastructures [27]. If nothing else, UAV photogrammetry has the capability to allow for the simplified visual inspection of a civil system [14]. Yet this research aims to outline all of the possible, practical, and useful ways UAV photogrammetry can be used to aid in the evaluation and condition assessment of civil infrastructure for effective maintenance.

2.4 Applications in civil engineering

Photogrammetric techniques have been used in civil engineering for a wide range of applications. These applications include crack detection, measurements of distortion, and structural deflections[20]. Unlike PCM produced from LiDAR systems, photogrammetric invariance (sparse outliers) are very easily characterized due to the existence of a texture pattern showing the object visually.

Civil engineers currently use photogrammetric data to collect land surveying data. By using an unmanned aircraft vehicle (UAV) and the fully nadir collection of many photographs, a 3D terrain of a plot of land can be calculated [5].

Existing publications have gone as far as to show the use of ground penetrating radar (GPR) measurements to produce meaningful geometric data for modeling of masonry bridges in conjunction with photogrammetric techniques [32]. However, ground penetrating radar can not provide enough information to determine boundary conditions at the arch supports [31]. Photogrammetric techniques have also demon-

strated ability to automatically find and accurately locate the obstacles in the power line corridors with measurement accuracies better than 0.5 m [39], demonstrating an effectiveness for inspection. Furthermore, close range photogrammetric techniques have exemplified their usefulness as tools for conservation or restoration of culturally historic landmarks. Photogrammetry allows exhaustive analyses in terms of shape, size, existing materials, state of preservation, localization of most damaged areas,etc. [2]. One study conducted in Athens used a combined SFM and laser scanning method to construct a 3D model which could be used to determine the best method of support for a statue on display to meet both the aesthetic and structural considerations. The statue was constructed photogrammetrically and then converted into abaqus for finite element analysis [18].

There have even been successful structural engineering scenarios. For instance, a collapsed bridge in situ were shown to illustrate the effectiveness of the algorithms. The methodology accurately located elements of a collapsed bridge in the scene. These examples demonstrated the effectiveness of the methodology and its applicability to other structural engineering scenes [36]. With all of these capabilities in mind, civil engineers need to consider the most practical, and effective techniques to research. This research aims to provide 3D photogrammetric techniques which can be used to collect, organize calibrate, and effectively evaluate PCM for geometrically accurate visual inspection, data registration,and condition assessment of concrete structures and specimens.

Chapter 3

Methodology

The methodology through which analysis of point cloud models evaluated in this thesis can be classified into two distinctive categories, methodology of laboratory specimens (Figure 3.1) and methodology of in-situ structures (Figure 3.2.1). Each of which will be discussed in detail in this chapter.

3.1 Methodology of laboratory specimen

In this section the uses and acquisition strategies for photogrammetric laboratory specimens is elaborate.

3.1.1 Description of specimen

A total of 8 specimens were considered in this experiment. These specimens were chosen from past experiments conducted at UMass Lowell based on their geometrical, and visual characteristics. CN01, CND01,CN03 and CN04 were all cast with Quickrete® Type I Portland cement, all-purpose sand, and all-purpose gravel with a water-to-cement (w/c) ratio of 0.5 and a cement-to-sand aggregate ratio of 1:2:3. CN01 had an additional 0.475 ml of Darex® II AEA admixture. The square mortar panels PN01, PND01, and PND02 were all cast with Quickrete® Type I Portland cement and all-purpose sand. Mixed with w/c ratios between 0.35 and 0.55 and a

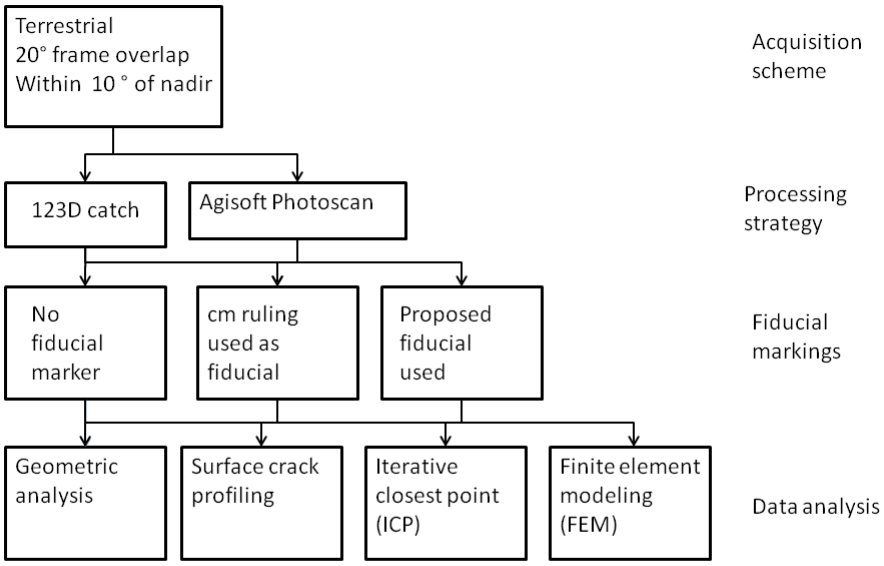

Figure 3-1: Flowchart for laboratory specimen methodology

sand to cement ratio of 2.53:1. These specimen are described in Table 3-1 and can be seen in Figures 3.1.1 through 3.1.1.

3.1.2 Laboratory setup and data acquisition

For all Lab specimen the data collection was nearly identical, while processing differed in camera used, number of photographs used, and processing softwares used. Two software packages were used in the processing or construction of the point cloud mod-

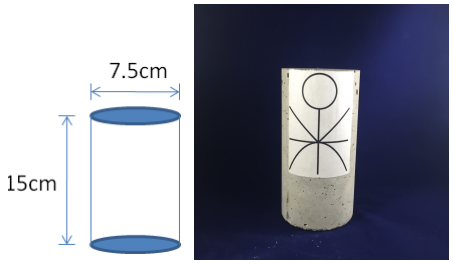

Figure 3-2: 7.5 cm x 15 cm cylinder; CN01

Figure 3-3: 10 cm x 20 cm cylinders; (left to right) CN02, CN03, CND01, CN04

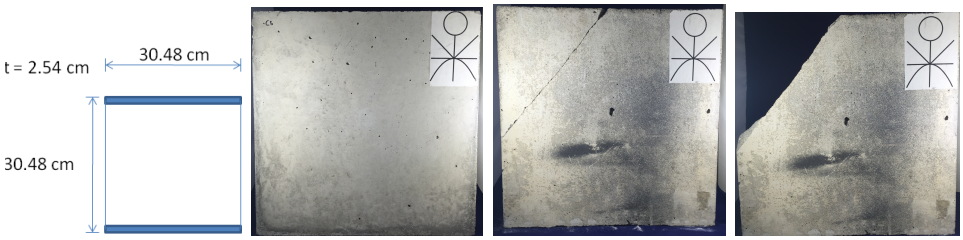

Figure 3-4: 30.48 cm square panels 2.54 cm thick; (left to right) PN01, PND01, PND02

Table 3.1: List of concrete laboratory specimens

Name	**Acronym**	**Description**
Cylinder 1	CN01	7.5cm x 15cm intact concrete cylinder
Cylinder 2	CN02	10cm x 20cm intact concrete cylinder
Cylinder 3	CN03	10cm x 20cm intact concrete cylinder
Cylinder 4	CN04	10cm x 20cm intact concrete cylinder
Damaged cylinder 1	CND01	10cm x 20cm concrete cylinder
Panel 1	PN01	30.48cm x 30.48cm x 2.54cm Intact concrete panel
Damaged panel 1	PND01	30.48cm x 30.48cm x 2.54cm cracked panel concrete panel
Damaged panel 2	PND02	30.48cm x 30.48cm x 2.54cm damaged concrete panel

Table 3.2: Processing strategy and analysis of each laboratory specimens

	Agisoft	**123D Catch**	**Fiducial used**	**GA**	**SCP**	**ICP**	**FEM**
CN01	x	o	x	x	o	o	o
CN02	x	o	x	x	o	o	o
CN03	x	o	o	o	o	x	o
CN04	o	x	o	x	o	o	o
CND01.2	x	o	x	x	x	o	o
CND01.1	o	x	o	x	x	o	o
PN01	x	o	x	x	o	o	o
PND01	x	o	x	x	x	o	o
PND02	x	o	x	x	x	o	o

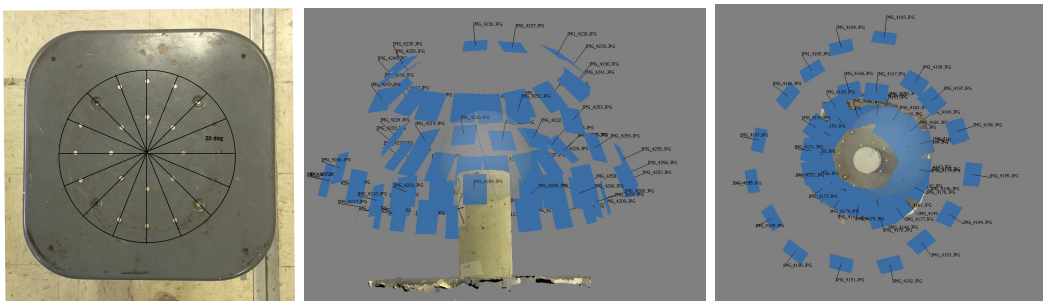

Figure 3-5: Frame overlap and data acquisition

els discussed in this chapter. Some of the models were constructed using 123D catch, a free to use Autodesk software. Others were constructed using Agisofts photoscan.

Models constructed using Autodesks 123D Catch software include CN04, and CND01.1. These models were previously used to to conduct an initial analysis of point clouds for condition assessment [10].

Models constructed using Agisofts Photoscan software used a maximum of 64 photographs each. CND01 was remodeled in Agisoft and as such has two differently calibrated models associated with it. These models were used for a more in depth accuracy analysis of point cloud modeling for evaluating concrete specimens [11]

In all modeling scenarios the natural spacing of holes on a laboratory stool was used for acquisition distance between photographs, taken with a 20° rotation. The perspective angles of photographs taken were be kept within 10° of nadir. Too large of a perspective angle can lead to photographs containing misleading information for the photogrammetric construction algorithms used. Figure 3-5 shows the stool and the data acquisition scheme.

Models CND01 and CN04 were constructed using as many as 70 photographs a lower resolution camera (iPhone 4). CND01 was then reconstructed using Agisoft's Photoscan for the second study. CN04 however had been marked with lines which would affect the algorithmic construction and add an additional parameter to be considered. It was preferred that models used in the second study be clear of markings aside from a proposed fiduicial (Figure 3-6).

Table 3.2 outlines the processing and analysis of each of the laboratory specimen

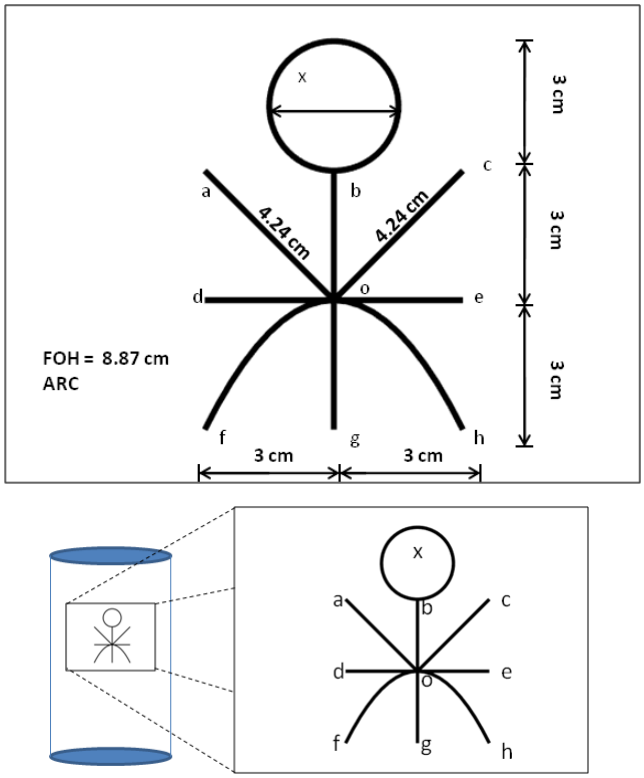

Figure 3-6: Proposed fiducial marker/calibration marker

which are discussed in this study. An (x) indicates a positive affirmation and (o) indicates a non-inclusion for each category. Figure 3-1 outlines a flowchart which exhibits all possible paths of laboratory specimen from acquisition to analysis. Although many different data collection strategies were used and all data was compared, discussion of accuracy was ultimately organized by independent parameters of the PCM such as PCD.

3.1.3 Geometric characterization

For geometric characterization using photogrammetry, length estimation (a straight line, a parabola, a circle), curvature estimation, area estimation, and volume estimation were applied in this research. Number of photos and PCD (or P) were used in quantifying the difference among various PCM. For length estimation, performance of various PCM was evaluated by

$$Er_L(\%) = \frac{1}{m}\sum_{i}^{n}\left(\frac{L_{PCM} - L_{act}}{L_{act}} \times 100\%\right)_i \tag{3.1}$$

where $Er_L(\%)$ = average error in length estimation (%), m = number of data points, L_{PCM} = estimated length using PCM, L_{act} = actual length measured by the fiducial marker. For curvature estimation, radius of curvature (ρ) was used and defined by

$$\rho = \frac{\left[1 + \left(\frac{dy}{dx}\right)^2\right]^{3/2}}{\left(\frac{d^2y}{dx^2}\right)} \tag{3.2}$$

The performance of curvature estimation was determined by

$$Er_\rho(\%) = \frac{1}{m}\sum_{i}^{m}\left(\frac{\rho_{PCM} - \rho_{act}}{\rho_{act}} \times 100\%\right)_i \tag{3.3}$$

where $Er_\rho(\%)$ = average error in length estimation (%), m = number of data points, L_{PCM} = estimated length using PCM, L_{act} = actual length measured by the fiducial

marker.

For area estimation,

$$Er_A(\%) = \frac{1}{m}\sum_{i}^{m}\left(\frac{A_{PCM} - A_{act}}{A_{act}} \times 100\%\right)_i \tag{3.4}$$

where $Er_A(\%)$ = average error (%), A_{PCM} = estimated area using PCM, A_{act} = actual area measured by the fiducial marker. For volume estimation, the volumes of CN01,CND01, PND01, and PND02 were calculated photogrammetrically as well as by Archimedes displacement principle. The specimens were all submerged into a full water container of known volume and mass. The amount of displaced water was used to estimate volumes physically. Volumes calculated by water displacement were then compared to the volumes calculated by the PCM. Errors in volume estimation were computed by

$$Er_V(\%) = \frac{V_{PCM} - V_{act}}{V_{act}} \times 100\% \tag{3.5}$$

where $Er_V(\%)$ = error in volume estimation (%), V_{PCM} = estimated volume using PCM, V_{act} = actual volume measured by water displacement.

3.1.4 Surface crack profiling

The practical advantage to constructing a geometrically accurate photogrammetric model of a specimen or structure is the ability to conduct an optical or visual inspection at anytime. In this experiment, PCM were used to conduct surface crack profiling. The technique shown here exemplifies how these models can be used to easily identify, process, extract, and evaluate surface crack information which enables civil engineers to estimate material strength (or structural stiffness) reduction.

All estimated crack lengths (L_{PCM}) were calculated by the sum of the distances between each line using a raw data imported into a Matlab code, using Eq.(3.6).

$$L_{PCM} = \sum_{i=2}^{n}\sqrt{[(x_i - x_{i-1})^2) + (y_i - y_{i-1})^2 + (z_i - z_{i-1})^2]} \tag{3.6}$$

where L_{PCM} = estimated crack length using selected points, (x_i, y_i, z_i) = Cartesian coordinates of the i-th point, and $(x_{i+1}, y_{i+1}, z_{i+1})$ = Cartesian coordinates of the $(i+1)$-th point.

3.1.5 Mechanical property

Mechanical property (strain components) of concrete was investigated by subjecting a plain concrete cylinder to a compression test using an Instron Material Testing System in the Department of Civil and Environmental Engineering at UMass Lowell (Figure 4-15). Once the cylinder was loaded, photographs of the cylinder were taken at various aspect angles for photogrammetric modeling. The concrete cylinder was modeled at 0%(unloaded), 20% and 40% of its ultimate load (estimated to be 3,750 psi). The 20% and 40% loads were approximated at 750 lb (3,336 N), and 1,500 lb (6,672 N).

Average surface strain components (ϵ_r, ϵ_θ, ϵ_z) at the midsection of the cylinder were calculated from axial/logitidunal deformation ΔL circumference length s, and cross sectional area A from PCM.

$$\epsilon_z = \frac{\Delta L}{L_0} = \frac{L_i - L_0}{L_0} \tag{3.7}$$

$$\epsilon_\theta = \frac{\Delta s}{s_0} = \frac{s_i - s_0}{s_0} \tag{3.8}$$

$$\epsilon_r = \frac{\sqrt{A_i} - \sqrt{A_0}}{\sqrt{A_0}} \tag{3.9}$$

$$\tag{3.10}$$

where subscript 0 indicates the unloaded state of the cylinder and subscript i the loaded state of the cylinder. Diameter of the cylinder was also calculated by

$$d = 2\sqrt{\frac{A}{\pi}} \tag{3.11}$$

where d = diameter (cm) and A = cross sectional area (cm^2).

Table 3.3: Processing strategy and analysis of in-situ structures

	Agisoft	123D catch	Stitch	Insp	SAR	DIC	RBH	SCP	FEM
Lincoln st	o	x	x	x	x	x	x	x	o
Plain st	x	x	x	x	x	x	x	x	x
Pinanski	x	x	x	x	x	o	o	x	o
R.D.	x	o	o	x	x	o	o	x	o

3.1.6 Comparison with ICP

Performance of PCM was also assessed by comparing with ICP method that compares one PCM with another. ICP has been verified in literature for point cloud stitching using robotic kinematic information to estimate error on a relatively small surface in a laboratory setting [29] As well as for mapping using a robotic 3D mapper[3] Even in civil applications it has been used to stitch models together to test photogrammetric capabilities as a deflection, or strain guage measurement system [16].

PCM of unloaded (0%) specimen CN03 was used as the reference for all ICP comparisons. A maximum distance of 0.67872399 cm was used to represent the range of consideration from the reference PCM to other PCM. The ICP algorithm iteratively processed each point on the reference PCM and calculates the distance and number of points within this range. The 20% loaded PCM and 40% loaded PCM were each aligned manually (roughly) and then automatically (finely) to the unloaded, reference PCM. Once alignment was completed, each of the loaded PCM was evaluated for point clouds to determine distances (within a maximum distance of 0.6782399 cm) from the unloaded PCM. A Gaussian distribution function was applied for modeling the distribution of these distances.

3.2 Methodology of in-situ structures

3.2.1 Description of structures

In this study, two bridge locations in Lowell, Massachusetts as well as two locations on UMass Lowell's campus were used to construct 3D PCM for evaluation.

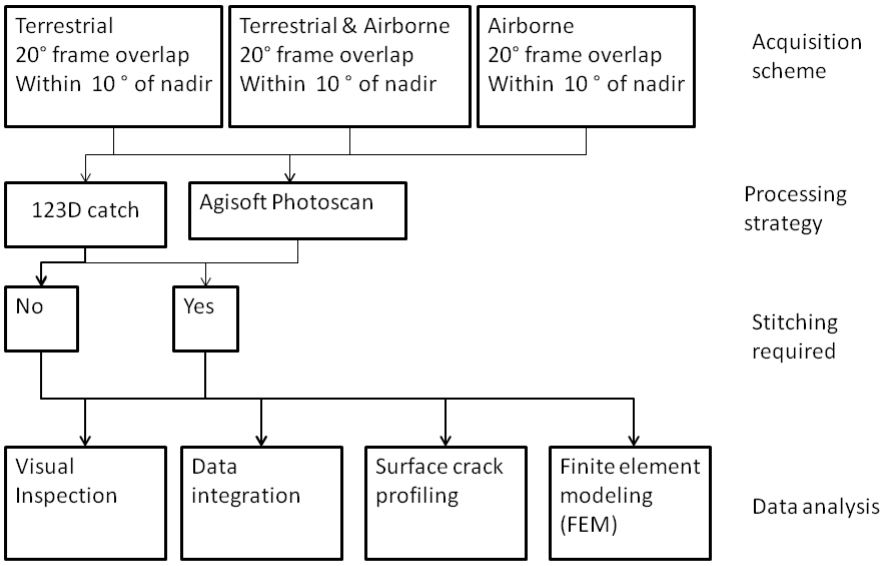

Figure 3-7: Flowchart for in-situ structures

3.2.2 Data acquisition strategy

The acquisition strategy for in situ structures is more complicated than the acquisition of laboratory specimens which was previously discussed. For a comprehensive model of a building or structure, a terrestrial and air-based acquisition strategy is presented. In some cases, the area of consideration does not require the use of a UAV. For instance, when modeling a wall or abutment that is relatively low (less than 10m). In these cases, terrestrial based acquisition schemes can be used. The acquisition should be done at several distances from the wall, with overlap of frames kept at approximately 20°. Perspective angles should once again be kept within 10° of the nadir or normal to the surface of interest. Figure 3-8 shows the data acquisition scheme for in-situ structures.

When conducting UAV acquisition, a video is recoded in 4K. The video is then disassembled into images using video editing software and taking interval screenshots based on the fps, and number of images required. It is important to pay atten-

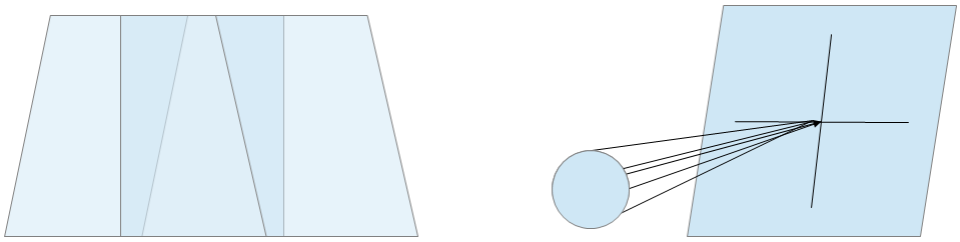

Figure 3-8: Data acquisition for in-situ structures

tion to frame overlap, and perspective angles in this regard. The more data under these constraints that is recorded, the easier it will be for the algorithm to construct a model. However, processing time also comes into consideration for these structures as well. When constructing full bridge or building models, it is important as a photogrammetric inspector to consider processing time. Models with too many procedural irregularities will take longer to process and may include noise based on confusing input data. Taking flight path, and flight time into consideration makes it easier when editing videos to convert the video into relevant image files.

3.2.3 Visual inspection

The most easily conceived and readily available use for point cloud modeling of civil infrastructure is the use in conjunction with professional engineers for visual inspection. Construction of a point cloud model gives an in depth, geometrically accurate and textured representation of the structure which can be viewed, saved, and compared easily. This research proposes that SFM PCM can construct models for use in visual inspection of bridges and buildings for structural health monitoring. Photogrammetric surveying takes relatively longer time and requires a more thorough analysis of the structure as no portion can be left unphotographed in order to achieve a geometrically accurate model and effective evaluation. In instances where UAV technologies are used for airborne acquisitions of data, a flight plan can be saved using autopilot functionality. By using autopilot functionality repeatability is vastly increased, and a best method can be established for any particular project.

3.2.4 Data registration

Construction of a geometrically accurate 3D PCM allow use of a global and local coordinate system which can serve as a way to organize and display data effectively. In this study, data from synthetic aperture radar (SAR), rebound hammer (RBH) and digital image correlation (DIC) experiments was integrated into PCM. This integration for comparison allows for comprehensive coordination, and a more effectively evaluated data.

3.2.5 Surface crack profiling

In a similar fashion to the surface crack profiling conducted on the laboratory specimen in this study, a surface crack profiling of in-situ structures was preformed. By conducting surface crack profiling analysis with a PCM, civil engineers can quantifying growing damages. Evaluation of the damage over time, as well as material strength can be inferred. Surface crack profiles were conducted on three in-situ locations discussed in the results section.

3.2.6 Finite element modeling

Since PCM are demonstrated to have high geometric accuracies, they can be imported to and used in finite element analysis. Although no finite element analysis was conducted in this research, the feasibility was evaluated. A PCM of one laboratory specimen (rebar) and one in situ example (column piece) were converted into a finite element model (FEM).

3.3 Data processing

In this study PCM were either processed using Autodesk 123D Catch, a one-step PCM construction algorithm. Alternatively, the PCM were first triangulated and captured as a normal or undense point cloud then reprocessed as a dense point cloud using Agisofts built in algorithm. The progression from point cloud, dense point cloud,

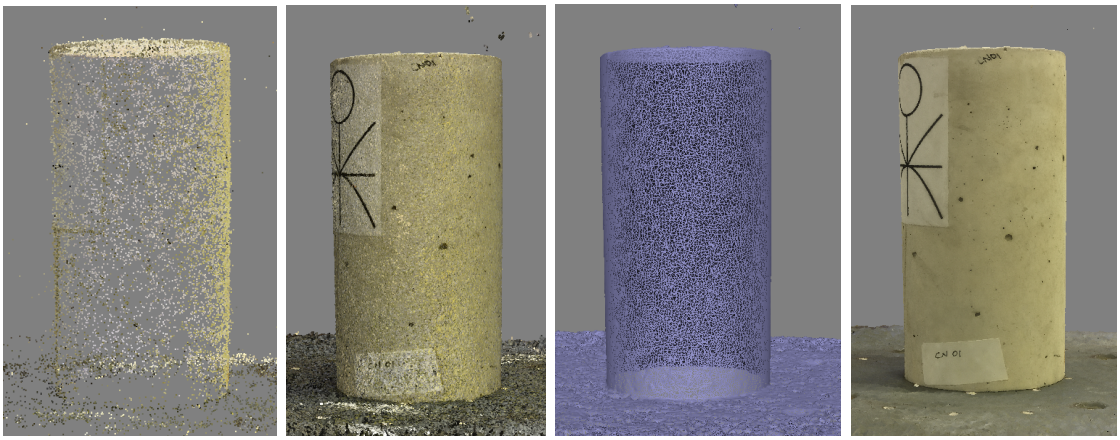

Figure 3-9: Progression of PCM construction

wire mesh, and finally textured model is shown in Figure 3-8. Upon completion of construction the models were exported as a 3D object .OBJ file to be sized, and re-sampled for further evaluation.

Chapter 4

Laboratory specimen results

Laboratory specimen results were used as the primary indication for accuracy ananlysis in effectively evaluating concrete specimen. As such, multiple studies were conducted. The first of which was preformed on models CND01 and CN04, whereas the second study included all models besides CN04. As CND01 was constructed using both softwares for two separate studies, it will be considered as both CND01.1 and CND01.2, where CND01.1 is the model constructed in the first, and CND01.2 the model constructed in the second study.

Models in the first study were calibrated to the smallest known length (the diameter of the cylinder) and subsequently evaluated for their ability to locate, and size lengths and locations of supposed known defects. The damaged specimen CND01.1 also underwent a cross sectional analysis which outlined how photogrammetry might be able to locate areas of high stress using extractable cross-sectional information.

Models in the second study were calibrated using the fiducial marker. Many more models were considered, including a smaller cylinder and two concrete panels. These models underwent a more stringent accuracy analysis, surface crack profiling and mechanical analysis which is discussed in full in the following sections.

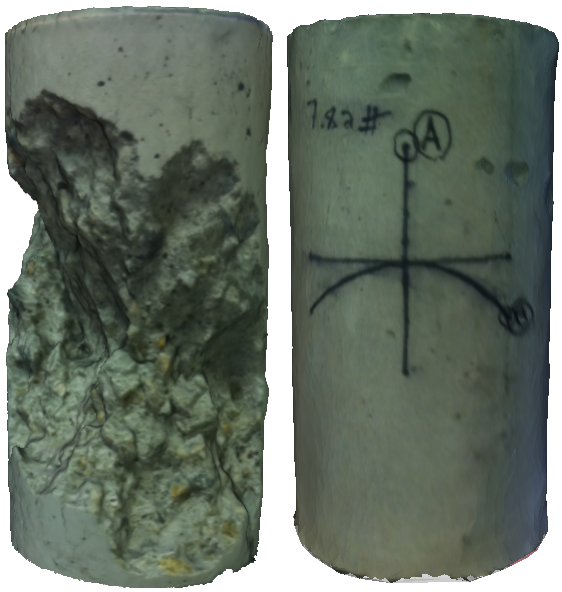

Figure 4-1: CN01.1 (left) shattered specimen & CN04 (right) intact specimen

4.1 Laboratory specimen results

4.2 Geometric characteristics

In order to trust PCM evaluation for concrete specimens and structures, two models were primaraly evaluated for their effectiveness in locating and identifying the size/severity of damages. Additionally, cross sectional evaluation on concrete specimens for the areas of high risk are define for stress mapping.

The two models, CND01.1 (shattered) and CN04 (intact) in (Figure 4-1) were modeled using the 70 and 64 photographs, respectively. Once the primary models were established, they were rendered at variant levels of photographs, and subsequently evaluated for their level of error with respect to photographs used to render. As the number of photographs decreases the level of overlap between image frames effectively drops and the quality of rendered models as a result, decreased proportionally. Models are defined with progressing roman numeral to express decreasing quality. The results are tabulated in Table A.1, graphed in Figure 4-3, and modeled using an exponential fit in Equations 4.1-4.3.

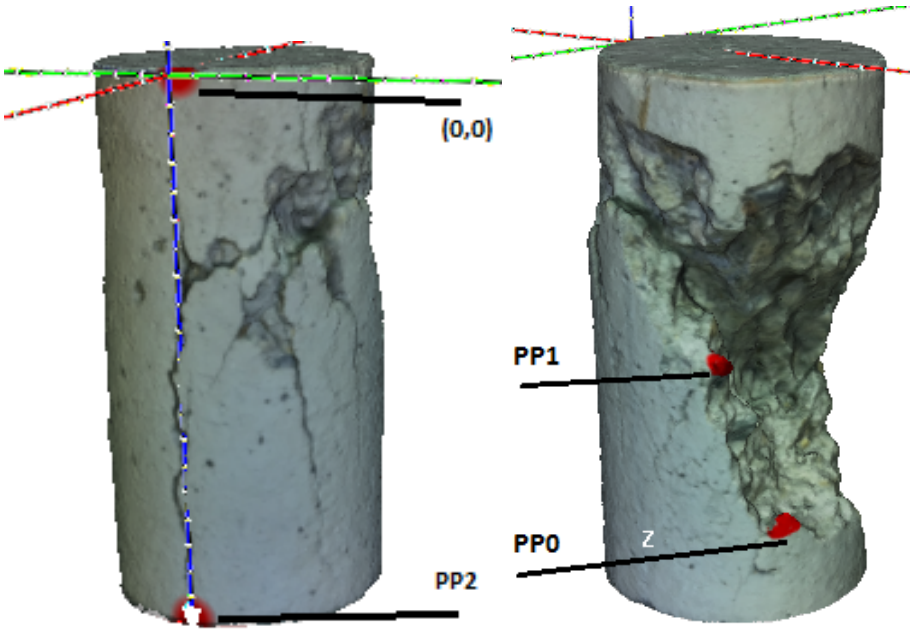

Figure 4-2: CND01.1 with Points PP0, PP1, PP2 for representative defects

4.3 Locating coordinates and defect sizes

Two concrete cylinder specimens were used. On CND01.1, the damaged concrete cylinder **PP1**, and **PP2** (x, y, z) were drawn placed on the specimen and then located photogrammetrically (Figure 4-2) . For this evaluation the origin was locally placed at a point easily recognized visually. The location of the origin was chosen to allow for easy localization of target areas both in real and point cloud modeling space. Out of the three points, **PP2** was placed on a straight path from the origin, **PP0** and **PP1** were placed on the far side of the cylinder to test the photogrammetric capability to account for dimensional changes in the x, y, and z directions. These three points as well as the origin, are represented by the red dots in Figure 4-2.

PP2 exhibited the least amount of error, as it was the closest to the origin and considered only translation in the z direction; at point (0, 0, 20). **PP0** and **PP1** located at (9.2, 3.5, 15.5) and (8.2, 4.6, 9.5), respectively, exhibited approximately the same amount of error as the degradation of the model continues. Yet, even at maximum deterioration, the locating ability of the photogrammetric techniques has a maximum error of only 6.275% on Model 1-V which was unable to fully render.

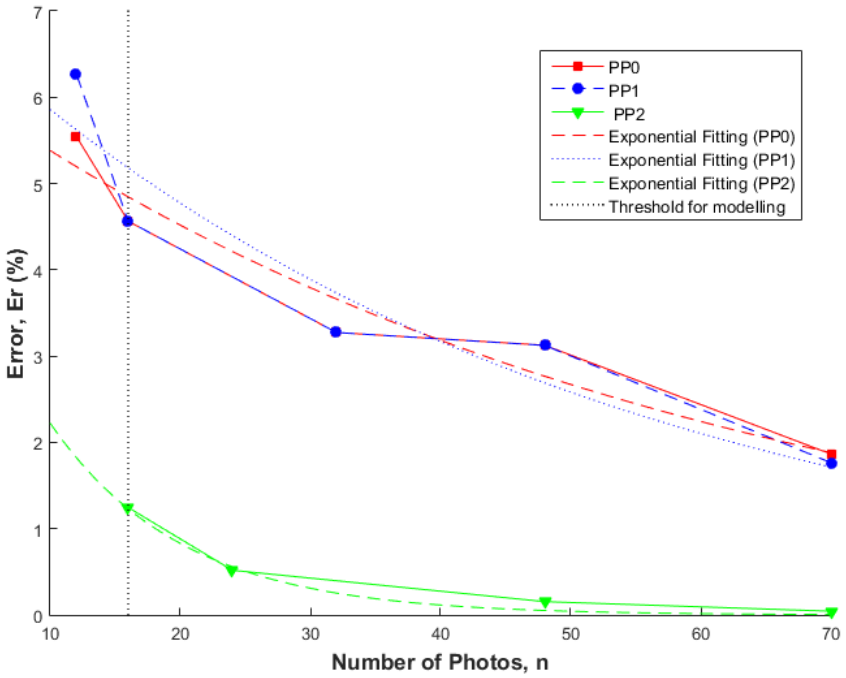

Figure 4-3: locating points on CND01.1 shattered cylinder

The results are graphed in Figure 4-3 the vertical dotted line represents the point at which the amount of photographs was not enough to construct a complete model. Errors with estimated coordinates of points **PP0**, **PP1**, and **PP2** were modeled by the fitted curves whose expressions are shown in (4.1), (4.2), and (4.3).

$$Er|_0^C(n) = 6.414\exp(-0.01751n) \tag{4.1}$$

$$Er|_1^C(n) = 7.191exp(-0.02048n) \tag{4.2}$$

$$Er|_2^C(n) = 5.962\exp(-0.0986n) \tag{4.3}$$

where $Er|_i^C$(n) = the error with respect to photographs taken in CND01.1-I

through CND01.1-V, and n = the number of photographs, Er = error, i = point considered PP(i), C= coordinates, and n=number of photographs

These results demonstrated that significantly less error is associated with the identification of a point which is only translated with respect to one direction than a point with translations in multiple directions. **PP2** which is located at (0, 0, 20) was identified with significantly less error than the other two points modeled.

The analysis for CN04 (intact specimen) focused on the accuracy in obtaining the length of a line or "size of defect" photogrammetrically. Whereas points are defined individually, a lines length is not only contingent on the points and known orientation but also the spaces in between. As such, lengths are generally more influenced by noise in photogrammetry [15]. Three lines were drawn on cylinder CN04, a straight line on a flat plane A, a curved line on a curved surface B, and a straight line on a curved surface C (Figure 4-4). The actual and photogrammetrically calculated lengths are tabulated in Table A.3. The Error of each line estimation with respect to photographs taken was tabulated in Table A.2, and graphed in Figure 6 in order to represent the effectiveness of the technique.

In Figure 4-5, as observed in the evaluation of Model 1, the trendline for CN04 shows a decreasing error as the number of photographs increases. This evaluation exhibited a maximum error of only approximately 4.4%, a reasonably low number for civil engineering applications. Line A or defect A, which was a straight line on a flat surface was expected to exhibit the lowest error, and exhibited less than 1% maximum error . Curiously the error in line B shot up as the number of photographs increased from CN04-II to CN04-III. This error was due to the complexity of measuring a curved line on a curved surface, as such this parameter (curvature) was further investigated in the second study. In order to nullify the effect of this outlier, the error in line B was modeled based on a more linear set of data. However, with all errors below 5% it is reasonable to consider the difference as negligible. Line B was in fact the most difficult line to calculate as it a curved line on a curved surface, exhibiting the most subjection to change. It had exhibited more error than not only the straight line on a flat plane A, but also more than C the straight line on the curved surface. A exhibited

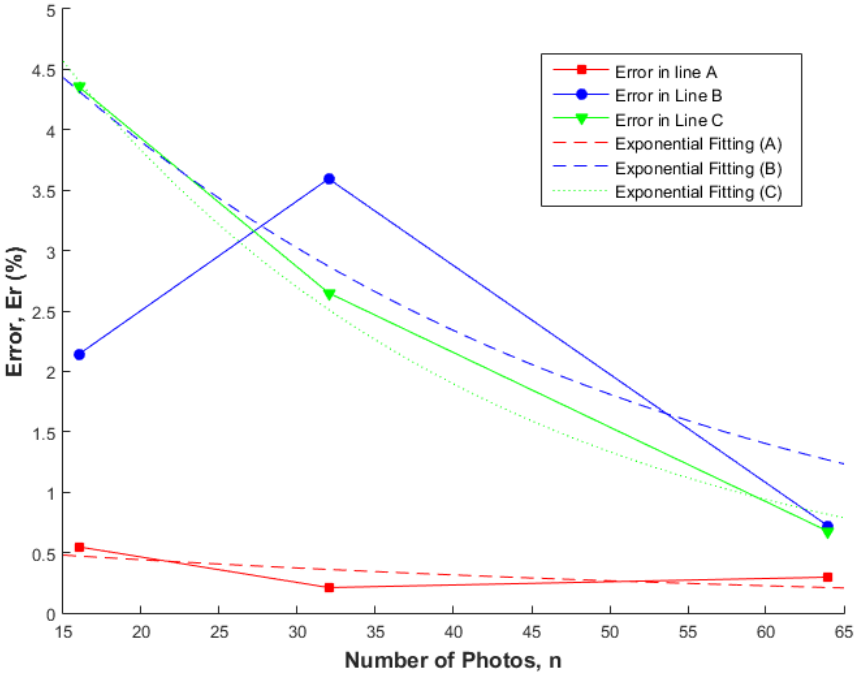

Figure 4-4: Length estimation error, on intact cylinder CN04

a significantly lower error, as the surface disparities did not come into effect. All line lengths were calculated, both physically, as well through the calculation of the sum of disparities of manually plotted points, using 13, 18, and 24 points for lines A, B and C, respectively. Error associated as a function of photographs are tabulated in A.2 and defined for all three lines in Equations (4.4), (4.5), and (4.6).

$$Er|_A^L(n) = 0.6161\exp(-0.01677n) \tag{4.4}$$

$$Er|_B^L(n) = 6.506exp(-0.02558n) \tag{4.5}$$

$$Er|_C^L(n) = 7.735\exp(-0.03515n) \tag{4.6}$$

where $Er|_i^L$(n) = the error with respect to photographs taken in Model 2-I through Model 2-IV, and n = the number of photographs. Er = error, i = defect considered line (i), L= length, and n=number of photographs. At this point, geometric characterization will be considered for the latter study.

In the second study, six PCM including CNDO1 (now considered CND01.2) were rendered with different numbers of photographs (64, 32, 22, and 17) and subsequently evaluated for their error with respect to multiple factors. Specimen CN03 was not considered in this section as it was used instead for mechanical load testing and was not given a fiducial marker. Figure 4-6 shows the average error in length estimation (Er_L) as a function of number of photographs (n). On the other hand, should the data points from specimen PN01 in Figure 4-6 be considered as an outlier, less than 3% of average error can be achieved in surface length estimation.

Average error in length estimation (Er_L) as a function of PCD (p) was investigated for all the specimens, as shown in Figure 4-7. In Figure 4-7, it was found that the average error reduces when PCD increases.

The average error (Er_L) with respect to PCD was modelled by Eq. (4.7) with an exponential function.

$$Er_L(p) = 11.62e^{-0.1287p} \tag{4.7}$$

where Er_L = average error in length estimation (%) and p = the PCD of a given

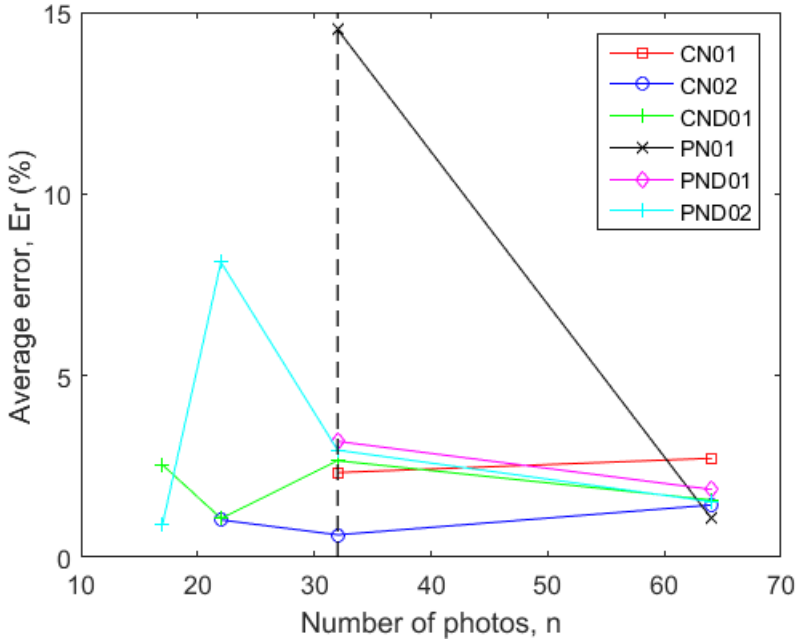

Figure 4-5: Average error Er_L with respect to photographs taken n

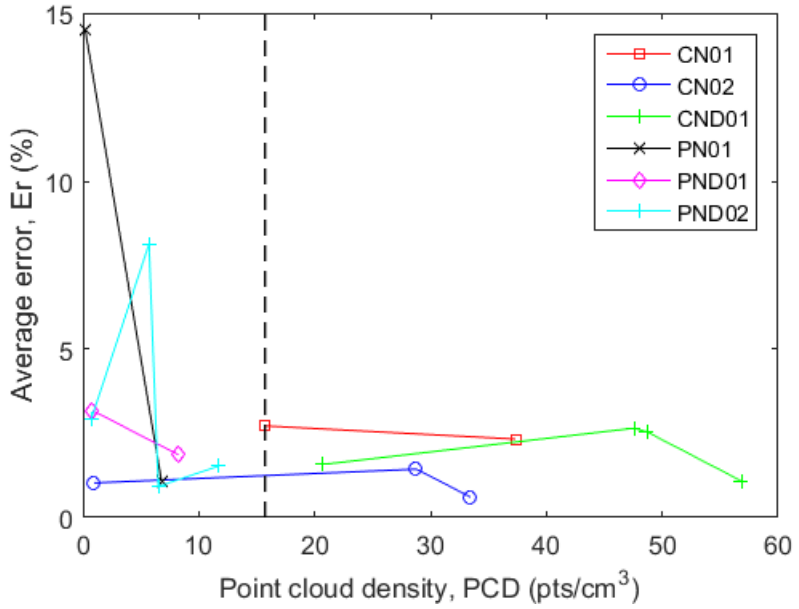

Figure 4-6: Average error Er_L with respect to PCD p

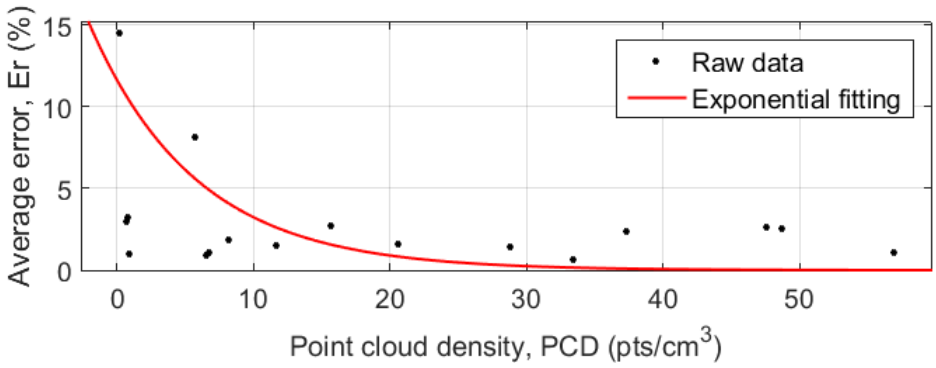

Figure 4-7: Average error Er_L with respect to PCD – Curve fitting

model (pts/cm^3). The stark difference in the accuracy declines exponentially with an increase in PCD as shown in Figure 4-8 Although the R^2 of Eq. (4.7) was as low as 0.5086, this correlation served to conceptualize the importance of PCD in all our PCM cases without any outliers. Therefore, PCD can be used for conducting an accurate account of reliability in photogrammetric modeling.

It was also found that damaged specimens were shown to exhibit less average error than intact specimens regardless of the geometry (Figure 4-9). Only damaged specimens were able to be rendered and evaluated with as few as 17 photographs. This finding suggests that SFM PCM will be much more easily rendered for damaged structures and specimens than for intact structures and specimens. The effect of radius of curvature (ρ) of specimens was investigated, as shown in Figure 4-10. Average error was plotted with respect to the inverse of radius of curvature ($\frac{1}{\rho}$). It was also observed that, although it seems conducive to compensate for curvature, further research should be carried out on other factors (e.g., surface texture, color contrast, light intensity).

The performance of the Laboratory specimen PCM was also considered for volume estimation. The level of error associated with the volume calculation of each of the considered models was calculated and illustrated in Table A.4 All errors remained under 5%.

Furthermore, a cross sectional analysis on damaged specimen, CND01 was used to evaluate its relative stress. The specimen was cut cross sectionally perpendicular

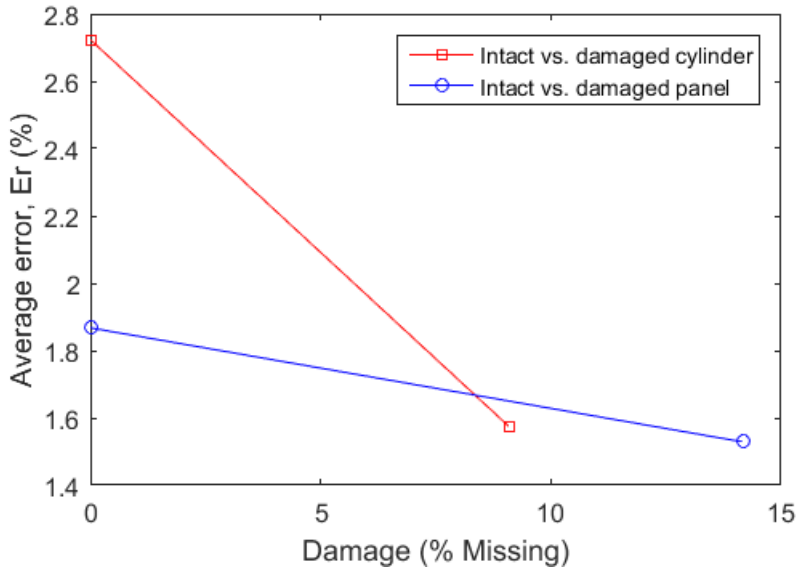

Figure 4-8: Average error in length estimation – Damaged vs. intact

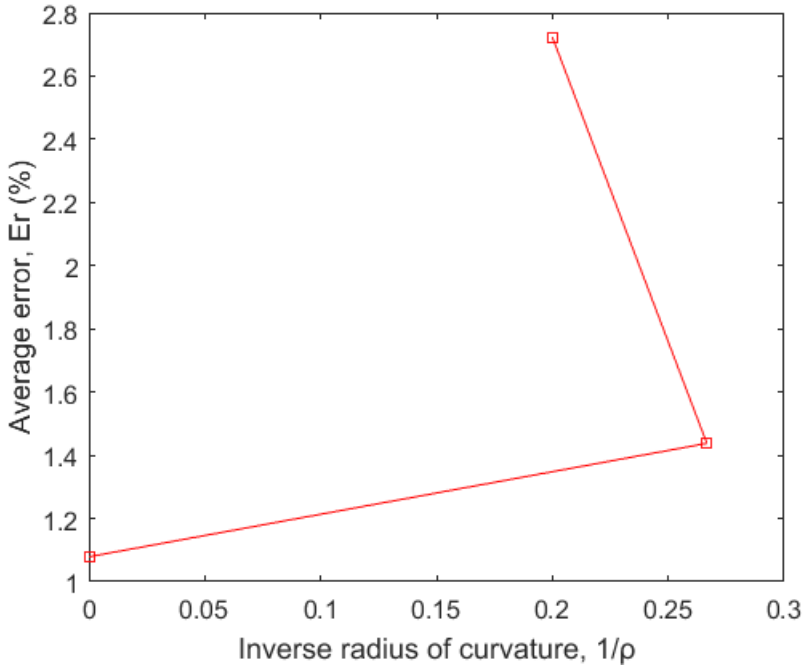

Figure 4-9: Average error with respect to inverse radius of curvature

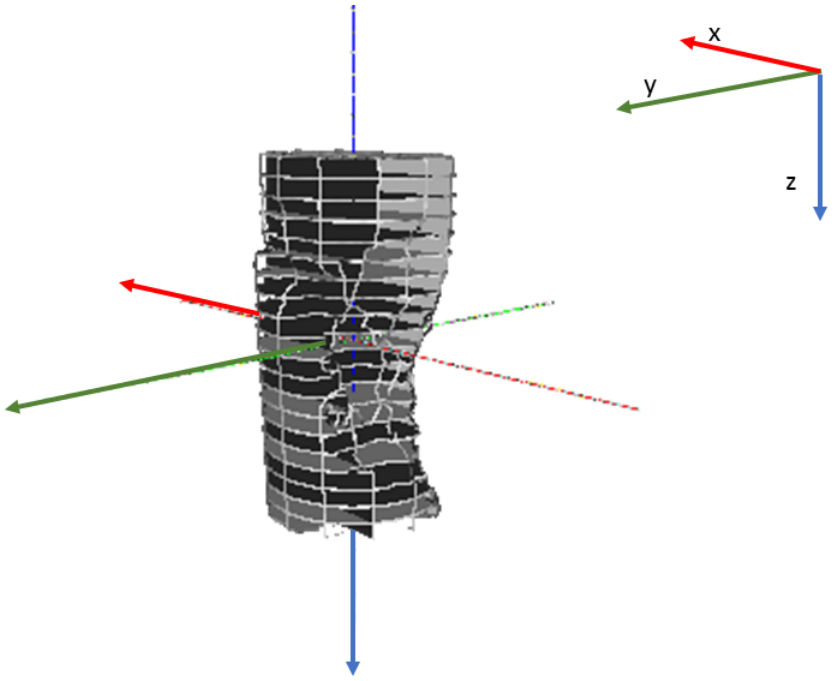

Figure 4-10: Cross sectional analysis of Model 1 (Shattered Cylinder)
Key: [Blue= z][Green = y][Red= x](Postive direction indicated in figure)

to the z axis at 21 locations with an increment $\delta z = 1$ cm from z= -10 cm through zero and up to z=10 cm. (Figure 4-11)

For the purpose of interpreting the experimental data, the cross sectional areas were normalized based on the difference in the error between the Meshlab and actual volumes. (Equation 4.8)

$$A^m_{z(adj)} = \left[1 - \frac{Er^m_1}{100}\right] \times A^m_z \tag{4.8}$$

where $\mathbf{A}^m_{z(adj)}$ = the adjusted cross sectional area, and $\mathbf{A}^m_z$ is the unadjusted cross sectional value obtain photogrammetrically. The Primary $\mathbf{A}^m_z$ and adjusted $\mathbf{A}^m_{z(adj)}$ cross Sectional areas are provided in Table A.3. Damage ($\mathbf{D}$) was calculated using an intact theoretical area $\mathbf{A}_{z(in)}$ and is defined (Equation 4.9)

$$D = \frac{(A_{z(in)} - A^{m}_{z(adj)})}{(A_{z(in)})} \times 100(\%) \tag{4.9}$$

Stress (σ) was calculated by applying a uniform load of 1 Newton to the cylinder. Cross sectional stress evaluation data is tabulated with corrections in Table A.6.

4.4 Surface crack profiling

Manual visual inspection typically involves locating cracks and damages. The demonstrated ability of PCM to exhibit information about cracking proves their viability for automated visual inspection. Figures 4-12 through 4-14 exemplify how the surface cracks can be profiled, extracted and evaluated. The lengths and widths of cracks on damaged specimen was calculated and can be seen Table A.5. These results prove the ability of PCM to estimate crack length and widths on the surface of concrete. Furthermore, this experimental procedure proves the ability of this information to be extracted and evaluated from PCM for specimens on an individual basis.

4.5 Mechanical properties

PCM were also evaluated for their ability to effectively evaluate the mechanical properties of specimens. Specimen CN03 was used for this portion of the study. Specimen CN03 does not contain a fiducial marker/calibration tool.

Four cross sections were calculated for specimen CN03 perpendicular to the z (axial) axis. The Surface area (SA) calculated from cross sectional information illustrated in Table A.7 and graphically displayed in Figure 4-16. These results exemplify the effects of the increase in mechanical loading. As the load increases so does the surface area.

Circumference data was also directly extracted from the PCM. This information is tabulated in Table A.8 and graphically displayed in Figure 4-17. Circumference was calculated as a length as in Eq. (3.6), and is thereby subject to error in calculation

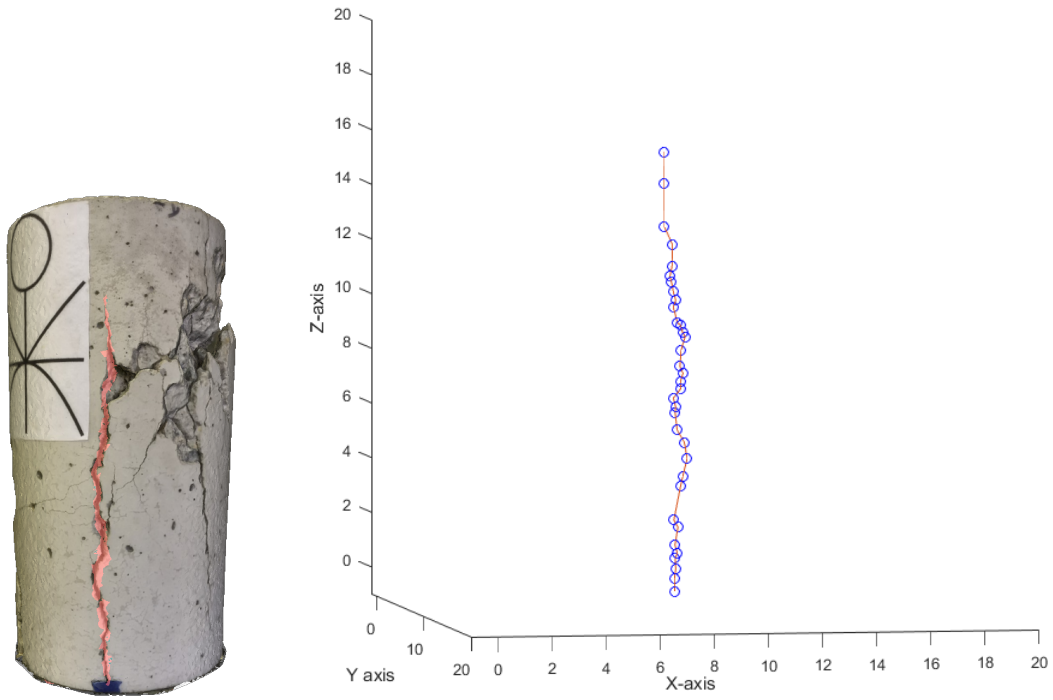

Figure 4-11: Cylinder crack 1 identification and extracted crack coordinates (cm)

unless the PCM used is infinitely dense. Because the differences in circumference in this example are so minimal, the trend-lines of these mechanically loaded specimen are not as expected. The 20% loaded specimen, appears to have a smaller circumference than the unloaded, whereas in the 40% loaded specimen it was found that the dilation effects outweighs the effects of the error in length calculation.

The Guassian distributions from the 20% and 40% ICP models are displayed with graphical color-scale representations of the distribution for further interpretation(Figures 4-18 and 4-19). In this ICP example the main comparison to be made is the mean distance which should correlate to lateral strain of the specimen. Due to the fact that the distance from each model to the unloaded was negative, the color scale in this example has an inverse representation. The more heavily loaded 40% specimen has almost two times the average error and is represented as the darker of the two models.

The increase in average iterative point distances provides data which can be correlated to the relative loading conditions of the specimen.

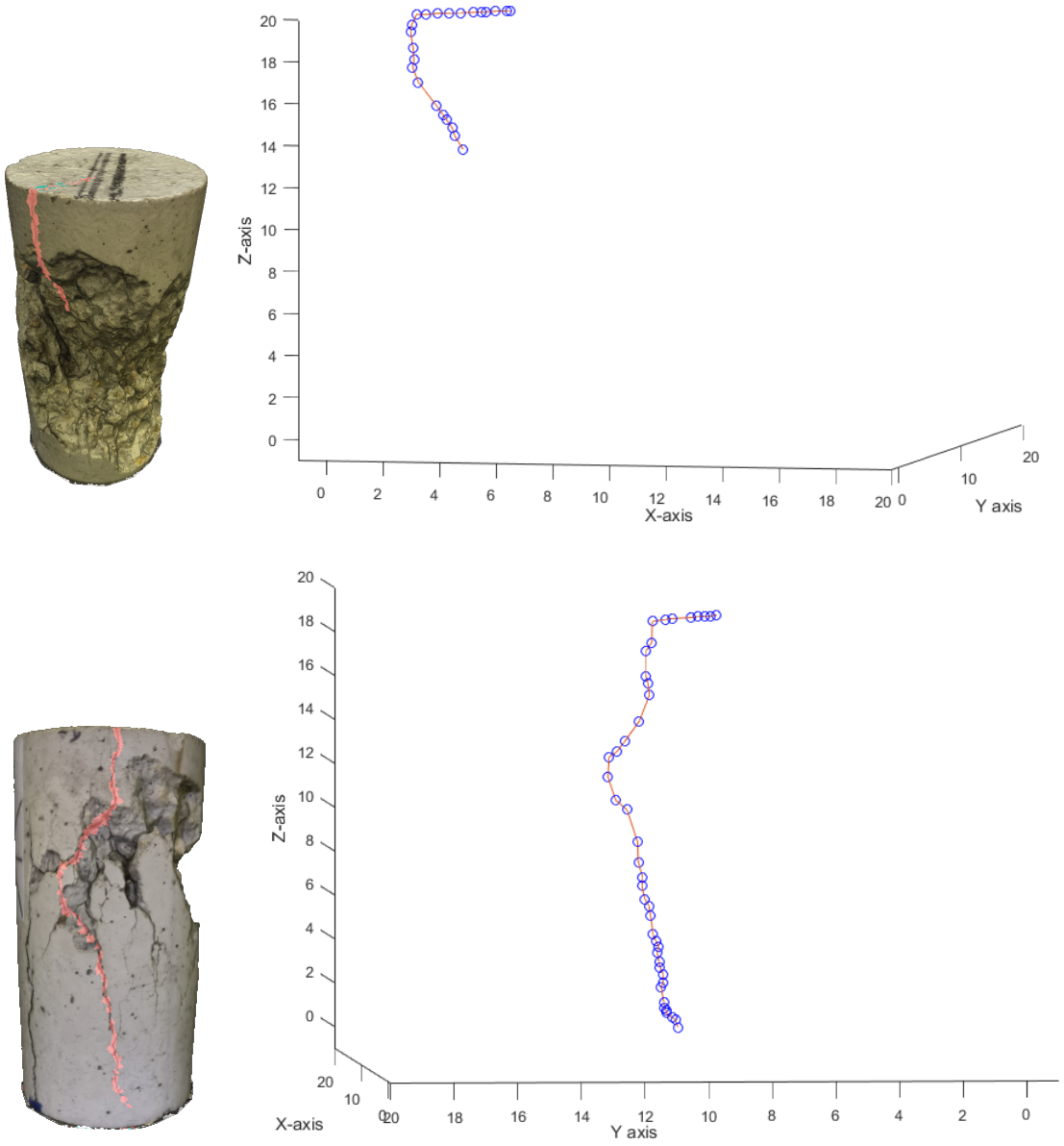

Figure 4-12: Cylinder cracks 2(top) and 3(bottom) identification and extracted crack coordinates (cm)

Table 4.1: Lateral strain at 20% and 40% loading using average diameter from surface area calculations

	0%)	**20%**	**40%**
Diam (d)**(cm)**	10.324654	10.36678	10.43731
Strain (ϵ_L)	N/A	0.00408	0.010911

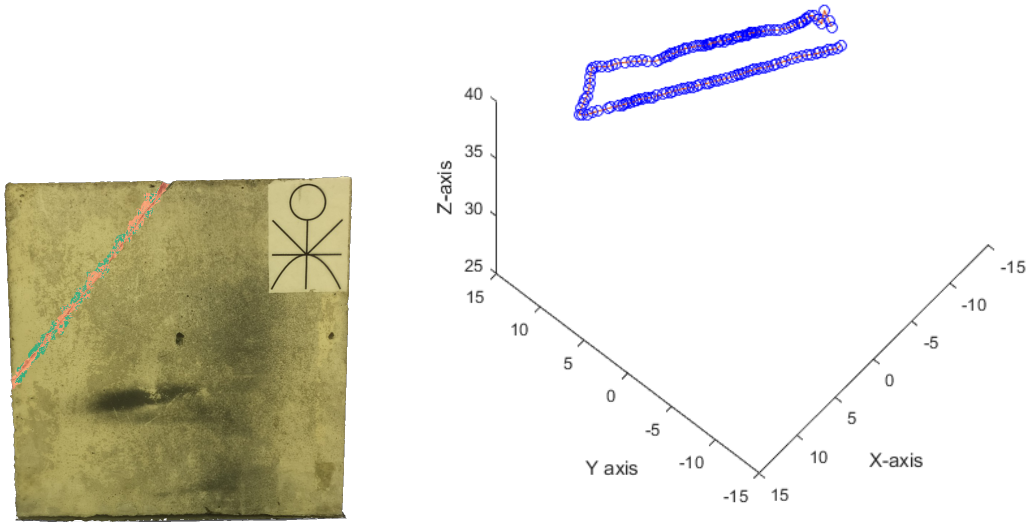

Figure 4-13: Panel crack identification and extracted crack coordinates (cm)

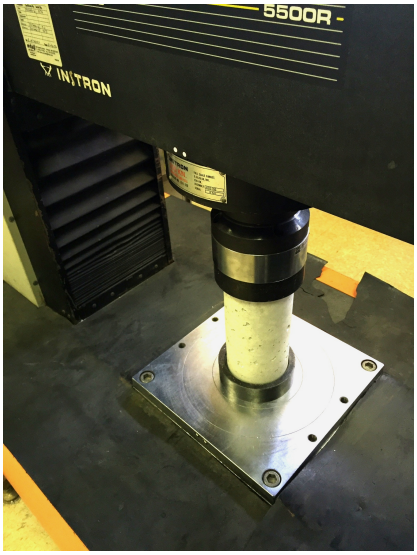

Figure 4-14: UMass Lowell's Instron material testing system

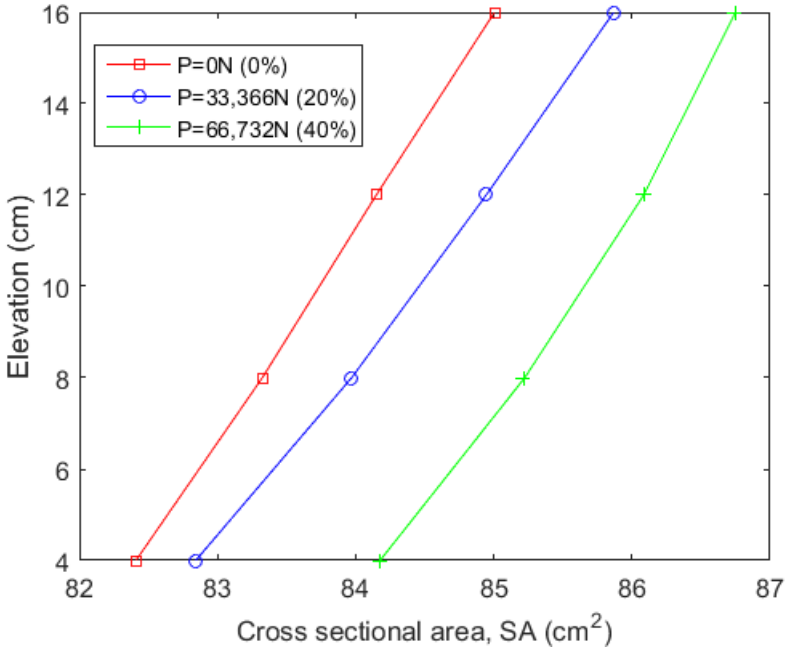

Figure 4-15: Surface area with respect to cross section

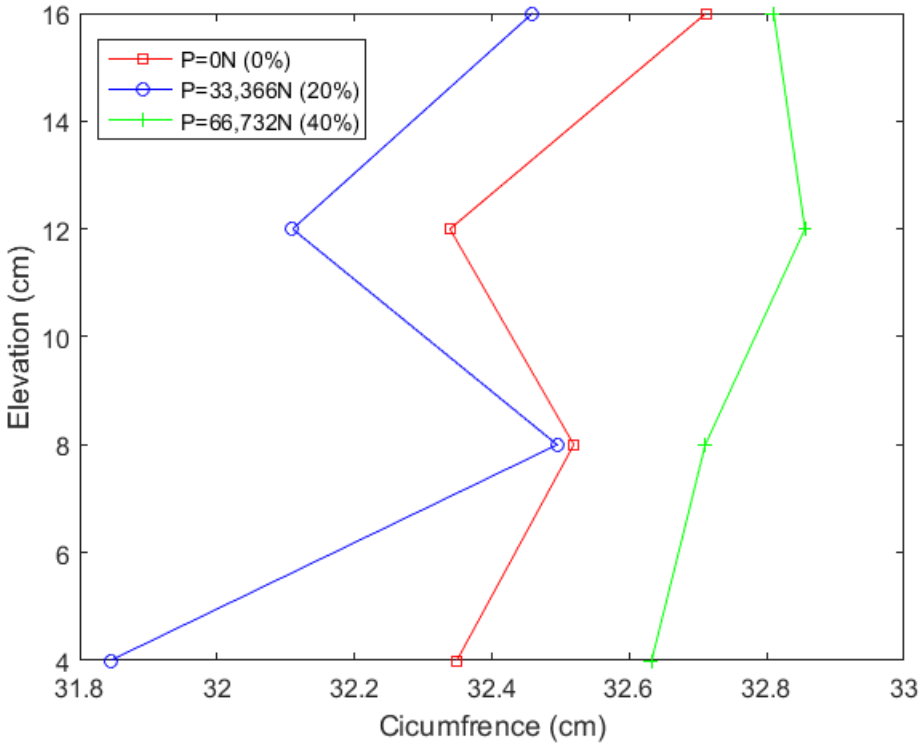

Figure 4-16: Circumference with respect to cross sections at different elevations

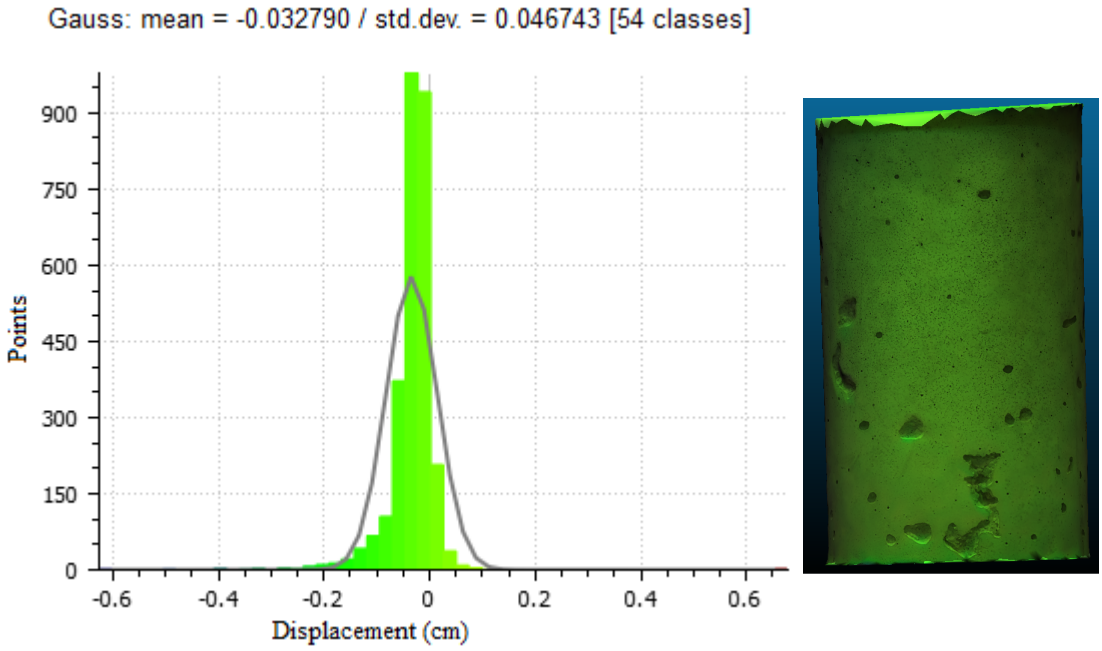

Figure 4-17: Iterative closest point results for 20% loading level

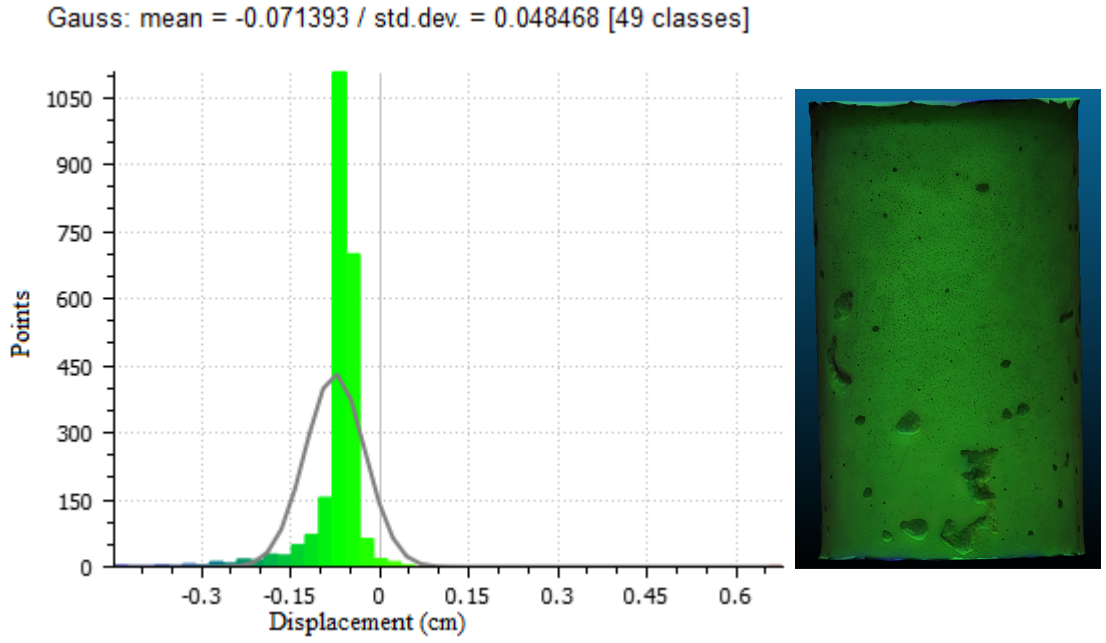

Figure 4-18: Iterative closest point results for 40% loading level

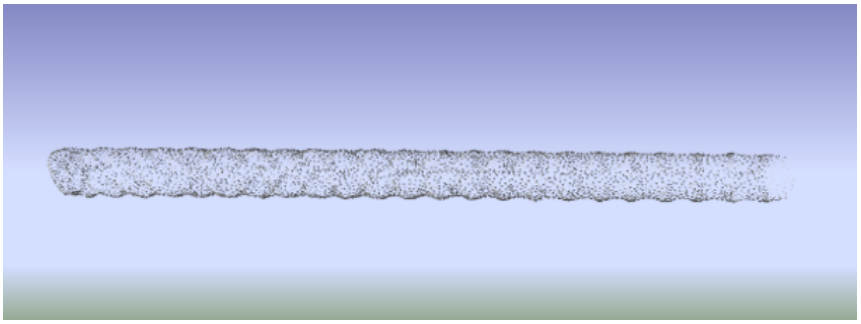

Figure 4-19: Original finite mesh

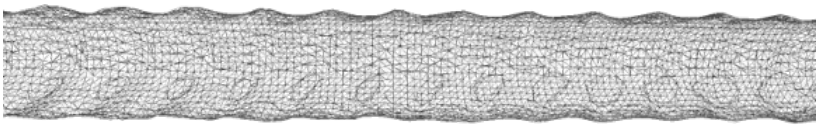

Figure 4-20: Re-sampled finite element mesh

4.6 Finite element modeling (FEM)

This section uses a rebar model constructed using uniform mesh sampling to show how civil engineers can use FEM constructed from photogrammetry to evaluate lab specimens.

Figure 4-20 shows a point cloud model as it was first constructed using the techniques described in 3.1.2 Laboratory setup and data acquisition. In order to be used effectively, the model must meet basic finite element requirements. It must be re-sampled to a uniform mesh grid (Figure 4-21), be closed, and be converted into an up-loadable format. The model was closed, and re-sampled using the "Merge Close Vertices" and "Uniform Mesh Resampling" filters which are included in Meshlab[8].

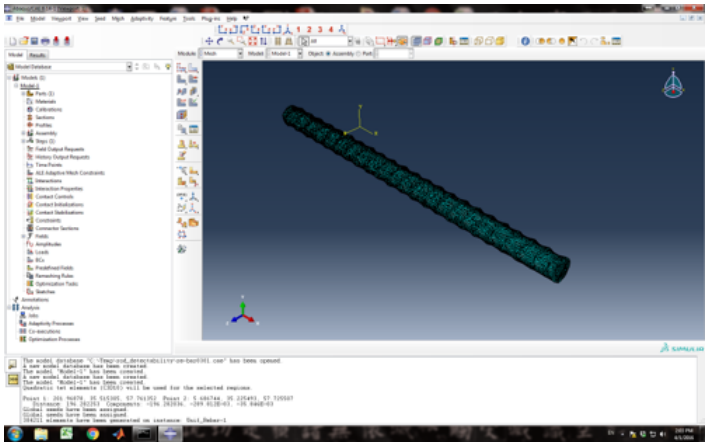

Figure 4-21: Screenshot of the finite element rebar model in Abaqus

They were subsequently converted from .stl into .sat format using a Matlab coding developed by a Adam H. Aitkenhead. After which the uniform mesh object was opened in Abaqus(figure 4-22). Although no finite element analysis was conducted, this research proved this technique is a viable strategy for FEM.

Chapter 5

In situ structure results

This chapter reports the results and analysis of photogrammetry on collected from various in-situ structures.

5.1 In-situ results

This section shows results not only as they pertain to the PCM themselves, but also UAV acquisition, and data collection.

5.2 Visual inspection

Current visual inspection techniques require on site inspection to be done by a trained professional engineer(PE). The case for the addition of photogrammetric models is an obvious one. Creating a 3D PCM requires the addition of only the time required to take pictures of the area of interest. This process requires the PE to be thorough in his examination, and makes for a re-countable piece of data which can be referred to overtime. The most beneficial of visual inspection models is comprehensive, in-situ structures, which encapsulates the entire structure of interest. Below are two full model examples which were used for several purposes but demonstrate the ability for 3D PCM to be used as visual inspection aids.Figure 5-1, which is a full building model of Pinanski hall, and Figure 5-2 which is a full bridge model of a bridge located

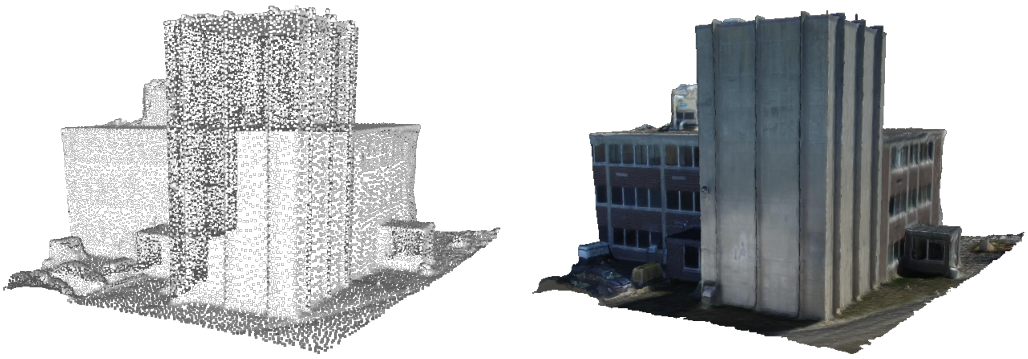

Figure 5-1: Pinanski visual inspection model

on Plain Street, Lowell Ma. Additional images for the Plain Street location can be found in B-1

5.3 Data registration

5.3.1 Synthetic aperture radar image registration

Among other new and emerging NDE techniques, SAR imaging can produce meaningful yet complicated results. Effects from geometry, material properties, and microwave diffraction can make for overly complicated and hard to read amplitude responses. In order to mitigate this, it is imperative that researchers, engineers, and scientists register SAR data into user-friendly models for their audience. SAR data registration is demonstrated in this thesis in three separate fashions. The first demonstrates in Figure 5-3, is the simple stitching of SAR data to an essentially flat wall from a fixed portable radar positioner at a receiving dock on UMass Lowells north campus. Addition images can be found in Figure B-2.

Second, Demonstrated in 5-4, a radar stitching to a protrusion on UMass Lowell's Pinanski hall which was used to demonstrate SAR response to geometric oddities. The measurements were taken from several heights using a fixed portable radar positioner. Additional images can be found in B-3.

Lastly, a demonstration of the ability to correct motion blurring of a SAR image

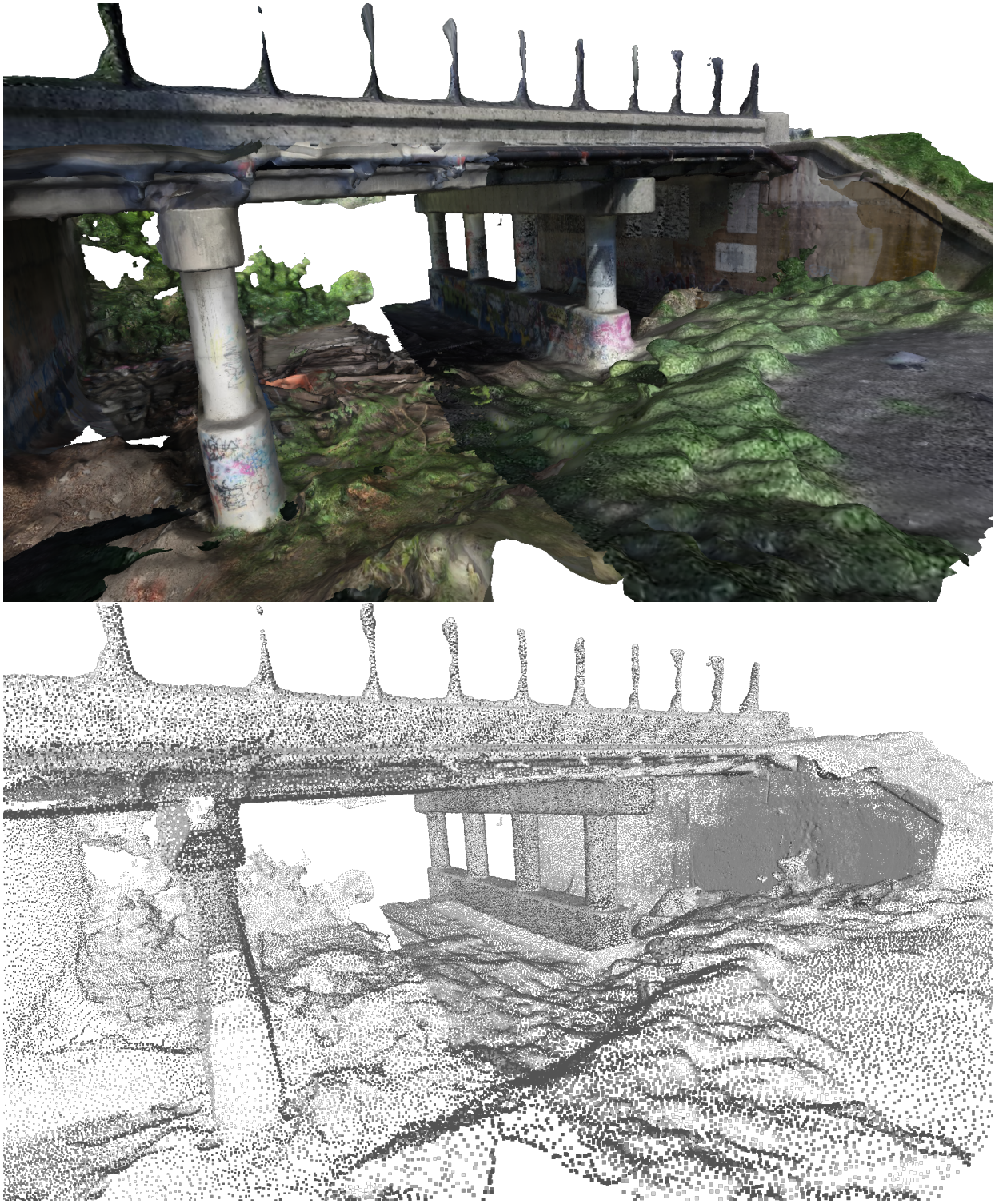

Figure 5-2: Plain Street bridge, Lowell MA. visual inspection model

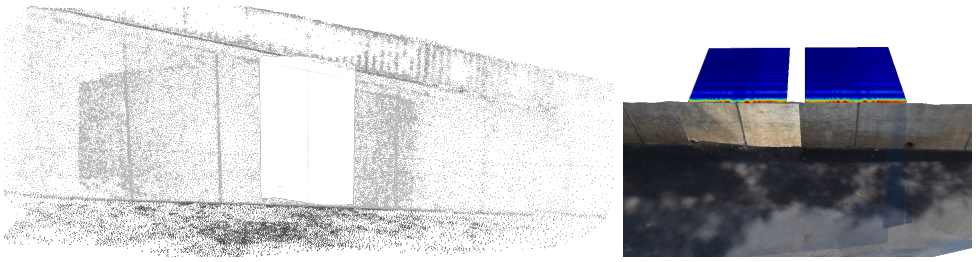

Figure 5-3: SAR integration at UMass Lowell's receiving dock

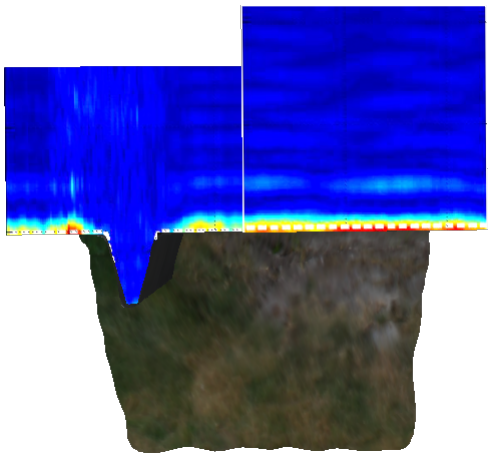

Figure 5-4: SAR integration at UMass Lowell's Pinanski Hall

Figure 5-5: Locations at which Photogrammetric motion compensation was conducted.

generated from a non-stationary SAR platform. Figure 5-5 shows the locations at which the measurements were taken for both SAR as well as photogrammetric data. Figures show the interpolation of the surface profiles. The interpolated surface profile was then mapped to interpolated data from the SAR image's maximum amplitudes to correct for motion effects in the image. The interpolated results are shown in Figure B-4. Where the first second and third rows of B-4, match up with the images on the left middle and right of 5-5 respectively.

5.3.2 Digital image correlation data registration

A comprehensive example is given in this section for the integration of DIC data into 3D PCM, seen in Figures 5-6 and B-5. While 3D PCM do have the capabilities to produce much of the same stress and strain information, they may lack in accuracy when compared with DIC. When available, DIC information may also be included and registered into the models. The example here is on a bridge abutment on Lincoln street in Lowell Ma. It focuses a total of four regions, and demonstrates how important stress and strain information can be analyzed more effectively. Stitching was done to include secondarily added DIC locations using Cloud compares ICP method. All DIC information was then manually integrated for evaluation.

5.3.3 Rebound hammer (RBH) data registration

Finally an example of RBH data on a Lincoln St. bridge abutment in Lowell, MA. is given in Figure 5-7 as well as B-6. This example includes complimentary SAR data.

Figure 5-6: DIC integration at Lincoln Street bridge, Lowell MA.

The SAR data was collected at three ranges, at each range, two scans were conducted. For each SAR resonse there is a RBH full data integration, and a spliced version to show the connection between the data sets. The side by side registration of the two sets of data allows for a more elaborately understood depiction of the health of the system under NDE invesitgation.

Point cloud modeling as shown above can make coordination amongs multiple NDE techniques much easier. It can also help provide a relative coordinate system onto which all NDE analysis can be preformed. The results above, indicate a virtual design process which is not only much easier to use as an engineer, but much more easily interpreted by managerial staff and employers. This shift into a more practical data analysis and display makes for the integration of these technologies much more feasible.

5.4 Surface crack profiling

In similar accordance to the procedure outlined for laboratory specimens, PCM of in-situ structures which are sufficiently dense, may also be used for surface crack profiling. In the following section two examples are given of in-situ surface crack profiling to demonstrate the capabilities of PCM for the analysis, quantification, and inspection of the progression of cracks on inspected in-situ structures.

The primary example is at the Lincoln Street bridge seen in Figure 5-8, and

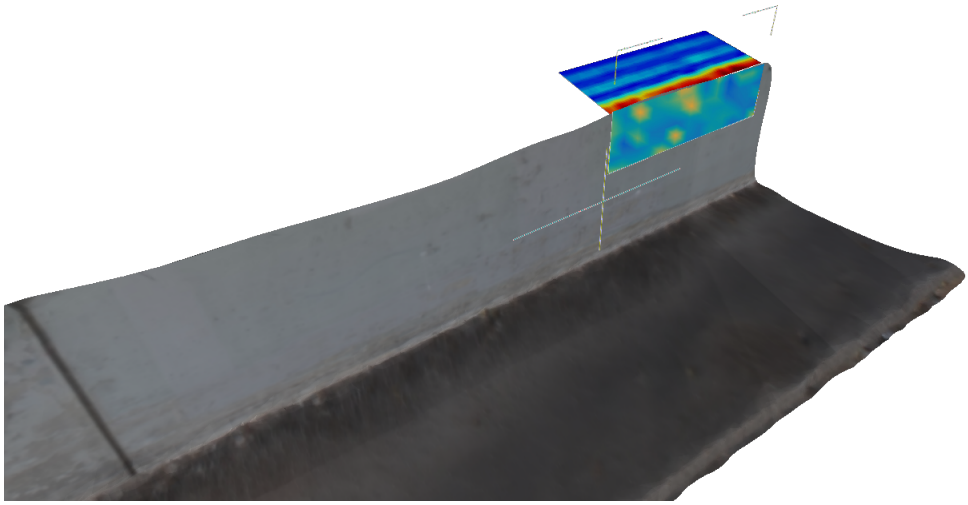

Figure 5-7: RBH/SAR integration at Lincoln Street bridge, Lowell MA.

Fibure B-7. Lincoln Street is the location of the abutment, which DIC information was recorded and integrated. The Second demonstration is a section of Pinanski Hall at UMass Lowell, and can be seen in B-8

5.5 Finite element modeling

To demonstrate the feasibility of converting PCM into FEM for finite element analysis, a section of the Plain street bridge shown in Figure 5-9 was cleaned by removing outliers and sectioning off open areas then it was re-sampled as a uniform grid. Once resampled into a uniform mesh, the .obj file was then converted to a .stl mesh using Meshlab. From there, a Matlab code was used to convert the file from a .stl to a .sat format. By converting the file from .stl to .sat, the file changes from a shell of infinitely small thickness (as only surface data is collected photogrammetrically) into a fully filled uniform mesh. .sat is a standard abaqus format, from which damaged

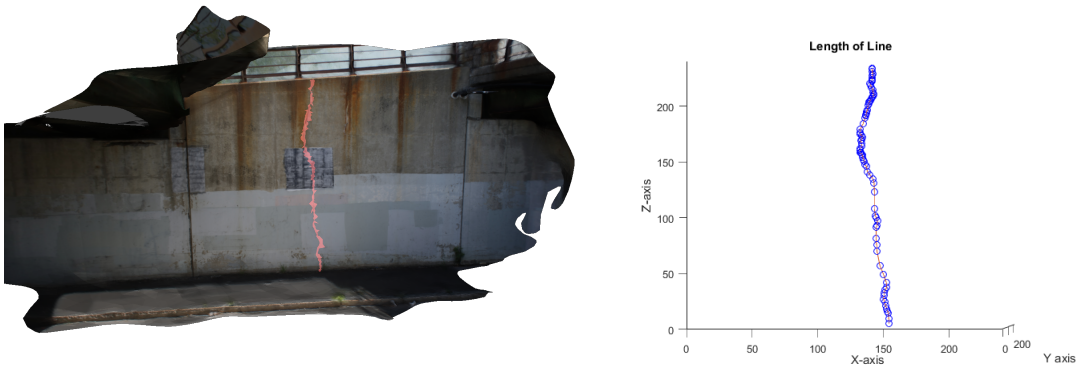

Figure 5-8: Surface crack profiling at Lincoln Street bridge, Lowell MA.

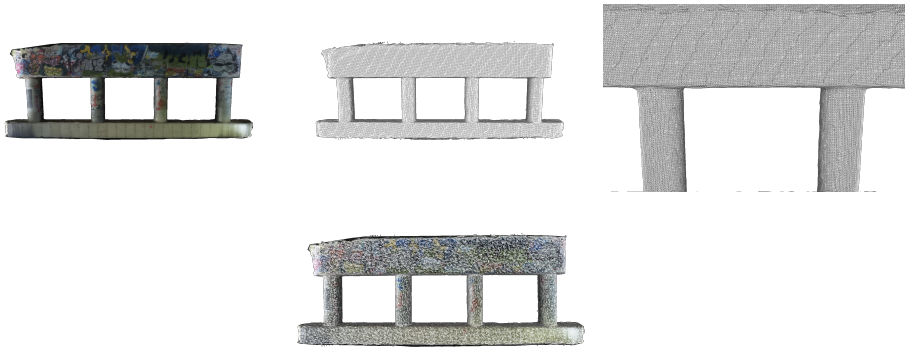

Figure 5-9: FEM from Plain Street bridge, Lowell MA. column section

and intact elements can be defined and evaluated. Once damaged areas are defined using photogrametric and other NDE techniques, a comparison of 'intact' to 'damaged' FEMs can be discerned allowing for the quantifiable account of the addition of damages on a structure. In instances where entire bridges and buildings are accounted for, this allows engineers to evaluate the health of the entire structure using a geometrically accurate model which incorporates all known surface, as well as subsurface (assuming the use of SAR) damages.

Chapter 6

Conclusion

The research presented in this Thesis aims to show the power and versatility of point cloud models for the evaluation of laboratory specimens as well as in-situ structures. The point cloud modeling approach used and discussed in this research is photogrammetry. Noting that a combination of both photogrammetry and laser scanning methods is currently the most comprehensive three dimensional virtual design coordination process conceivable. However, in this research, photogrammetry was the choosen tool for two reasons.

Firsts of all, photogrammetry is significantly less expensive than LiDAR or laser scanning equipment. As a researcher it is important to look for alternative ways to conduct your research which allow for repeatability and ease of use. Photogrammetry is a tool that is accessible to any person, anywhere, atno charge. From the research perspective, photogrammetry is an obvious choice. As part of this Thesis, a photogrammetric user manual located in appendix C was developed to outline the processes required for producing and analyzing relatively naive point cloud models. It is my sincerest hope that this information is presented in a user-friendly format to understand that any researcher, student, teacher, employee, or artist could produce meaningful results from these instructions. This would simply not be plausible if LiDAR or laser scanning was researched as it would have forced the research into a rather expensive niche.

Secondly, photogrammetry is a skillful and delicate approach and therefore re-

quires a more comprehensive understanding of optical surveying. When using a LiDAR or laser scanner for optical 3D surveying the user input required is fairly minimal when compared to photogrammetry. Photogrammetry requires a rather in depth understanding of the perspective invariance required to create an accurate point cloud model. An expert in photogrammetric construction will have little to no difficulty switching to a LiDAR scanning system. Therefore, it is much more worth-while to choose the photogrammetric approach.

6.1 Summary of major findings and results

- **Geometric characterizations**
  - External factors such as frame overlap, possible noise, and surface features, affect the general outcome of the PCM more significantly than the number of photographs taken.
  - Average error in length estimation generally decreases with the increase of the number of photographs. However, average error becomes large when the surface of target lacks of geometric feature (e.g., specimen PN01).
  - $n = 32$ photographs is used as a lower bound for length estimation with less than 5% error.
  - Number of photographs is not the primary factor affecting the performance of PCM and should not be used as the only parameter for assessing the performance (or accuracy) of PCM. Rather, other parameters such as PCD should also be considered as well.
  - A threshold PCD $p = 15.7194$ pts/cm^3 was proposed, corresponding to a 2.73% average error in length estimation in this study.
  - The effect of curvature is in fact not significant enough to outweigh other factors which determine the accuracy of PCM.
  - The volumes of PCM can be estimated with less than 5% of error)

- Damaged specimens are modeled more easily than intact specimens, SFM PCM will be much more easily rendered for damaged structures and specimens than they will be for intact specimens and structures.
- Photogrammetry can not only calculate the volume of a specimen or system, but also identify the critical section (the cross section with the highest stress) geometrically.

- **Surface crack profiling**
  - Point cloud modeling approach can deliver fully rendered structures, for visual inspection including surface crack profiling as demonstrated in Pinanski hall and Lincoln Street bridge model examples contained in this Thesis.
  - Lengths and widths of cracks can be plotted within the error with respect to a given model. Verified on laboratory specimen to be less than 3%.

- **Mechanical Property**
  - Mechanical properties including relative strain of a specimen loaded to different levels(20% and 40%) can be extracted from cross sectional area, measurements.
  - Strain calculations from direct circumference extraction is not recommended as it is subject to significant error.
  - The Gaussian distribution of average distance differences, calculated using iterative closest point method discussed in each loaded specimen as compared to the unloaded, can be used as a correlation to the level of strain and thereby the level of loading.

- **Data Registration**
  - Point cloud models can be used as a relative coordinate system as well as virtual design model for NDE integration and coordination.
  - Photogrammetry provides an approach/platform to integrate various NDE data such as SAR, DIC, and RBH.

- **Finite Element Modeling**
  - Although not fully functional, the feasibility of FEM for these models including NDE data was investigated by the developement ofFEmodels ofsteel rebar using photogrammetry..

6.2 Future research

The research conducted in the completion of this Thesis leaves for several future research opportunities. Suggested research includes. **1)** Continuation with FEM to produce more reliable models for mechanical analysis; **2)** Development of best method for SFM using UAV technologies; **3)** Best practice under the consideration of light source, in terms of both light source angle, perspective, and intensity; **4)** Continued integration of SAR data and other NDE/I/T; **5)** More mechanical studies using ICP methods outlined, especially deflection studies are recommended. Lastly, if possible a comparison with Lidar, or laser scanning methods. It is also suggested that educational demonstrations be prepared to teach civil engineering students how mechanical loads affect concrete specimens with the visual aid of photogrammetry.

Appendix A

Tables

Table A.1: Error in locating points CND01.1 (Shattered Specimen) (Model Vs Actual)

Model	**Number of Photos**	**Error PP0** (%)	**Error PP1(%)**	**Error PP2 (%)**
I	70	1.868	1.765	0.044
II	48	3.126	3.124	0.155
III	32	3.274	3.274	0.518
IV	16	4.563	4.563	1.245
V	12	5.549	6.275	N/A

Table A.2: Error in line lengths CN04 (Intact Specimen) (Model Vs Actual)

Model	**Number of Photos**	**Error line A(%)**	**Error line B(%)**	**Error line C(%)**
I	64	0.296	0.718	0.675
II	32	0.210	3.594	2.649
III	16	0.548	2.142	4.356
IV	12	N/A	N/A	N/A

Table A.3: Difference in line lengths CN04 (Model Vs Actual)

	Actual(cm)	**(I)(cm)**	**(II)(cm)**	**(III)(cm)**	**(IV)(cm)**
A	7.5	7.4777	7.446	7.551	N/A
B	9.1	9.119	8.773	8.859	N/A
C	10	10.055	10.214	10.436	N/A

Table A.4: Volume calculations and errors associated

Volumes	**PCM (cm^3)**	**Water Displacement (cm^3)**	**Error (%)**
CN01	1525.035	1570.00	2.864013
CN04	1525.034	1570.8	2.913547237
CND01	1436.947	1369.848	4.898281
PND01	2474	2380	3.94958
PND02	2124.0222	2150	1.208269

Table A.5: Crack length and width estimations of specimens CND01 and PND01 (Unit: cm)

	Total length	**Avg length**	**Avg width**
CND01-64	21.3694	7.123133	0.114904
PND01-64	52.8676	52.8676	0.02533

Table A.6: Cross sectional stress evaluation CNDO1

Z(coordinate)	$\mathbf{A}_z^m$ (cm^2)	$\mathbf{A}_{z(adj)}^m$ (cm^2)	$\mathbf{A}_{z(adj)}^m$	σ **(Stress)(Pa)**	**Damage(%)**
Z(-10)	37.915	36.057	0.0036	277.334	54.090
Z(-9)	83.058	78.989	0.00789	126.59	-0.572
Z(-8)	82.635	78.587	0.00785	127.247	-0.0602
Z(-7)	80.877	76.916	0.00769	130.011	2.0674
Z(-6)	77.521	73.723	0.007	135.642	6.132
Z(-5)	73.834	70.217	0.007	142.415	10.5963
Z(-4)	71.978	68.451	0.006	146.088	12.844
Z(-3)	71.090	67.608	0.00676	147.91	13.918
Z(-2)	66.988	63.707	0.00637	156.969	18.8861
Z(-1)	65.587	62.375	0.00623	160.320	20.581
Z(0)	63.394	60.288	0.00602	165.868	23.237
Z(1)	60.107	57.163	0.00571	174.938	27.218
Z(2)	59.124	56.228	0.00562	177.848	28.409
Z(3)	61.458	58.447	0.00584	171.0936	25.582
Z(4)	63.457	60.348	0.00603	165.703	23.161
Z(5)	65.957	62.726	0.006272	159.421	20.133
Z(6)	69.616	66.205	0.006	151.044	15.704
Z(7)	74.379	70.736	0.00707	141.371	9.936
Z(8)	77.147	73.368	0.00733	136.299	6.584
Z(9)	80.250	76.32	0.00763	131.0284	2.827
Z(10)	68.090	64.75	0.00647	154.428	17.551

Table A.7: Cross sectional areas, SA at 0%, 20%, and 40% loading levels

	0% (cm^2)	**20% (cm^2)**	**ΔSA(%)**	**40% (cm^2)**	**ΔSA(%)**
Z4	82.409714	82.84245	0.525097	84.17691	2.144403
Z8	83.3246	83.97095	0.775698	85.2244	2.279994
Z12	84.149651	84.94586	0.946185	86.08547	2.300448
Z16	85.00502	85.86791	1.015107	86.75012	2.05294
Avg	83.722246	84.40679	0.817638	85.55922	2.194134

Table A.8: Circumference values at 0%, 20%, and 40% loading levels (cm)

	0%	**20%**	**40%**
Z4	32.3490	31.8448	32.6327
Z8	32.5192	32.4950	32.7106
Z12	32.3389	32.1098	32.8556
Z16	32.7118	32.4592	32.8102
Avg	32.47973	32.2272	32.75228

Appendix B

Figures

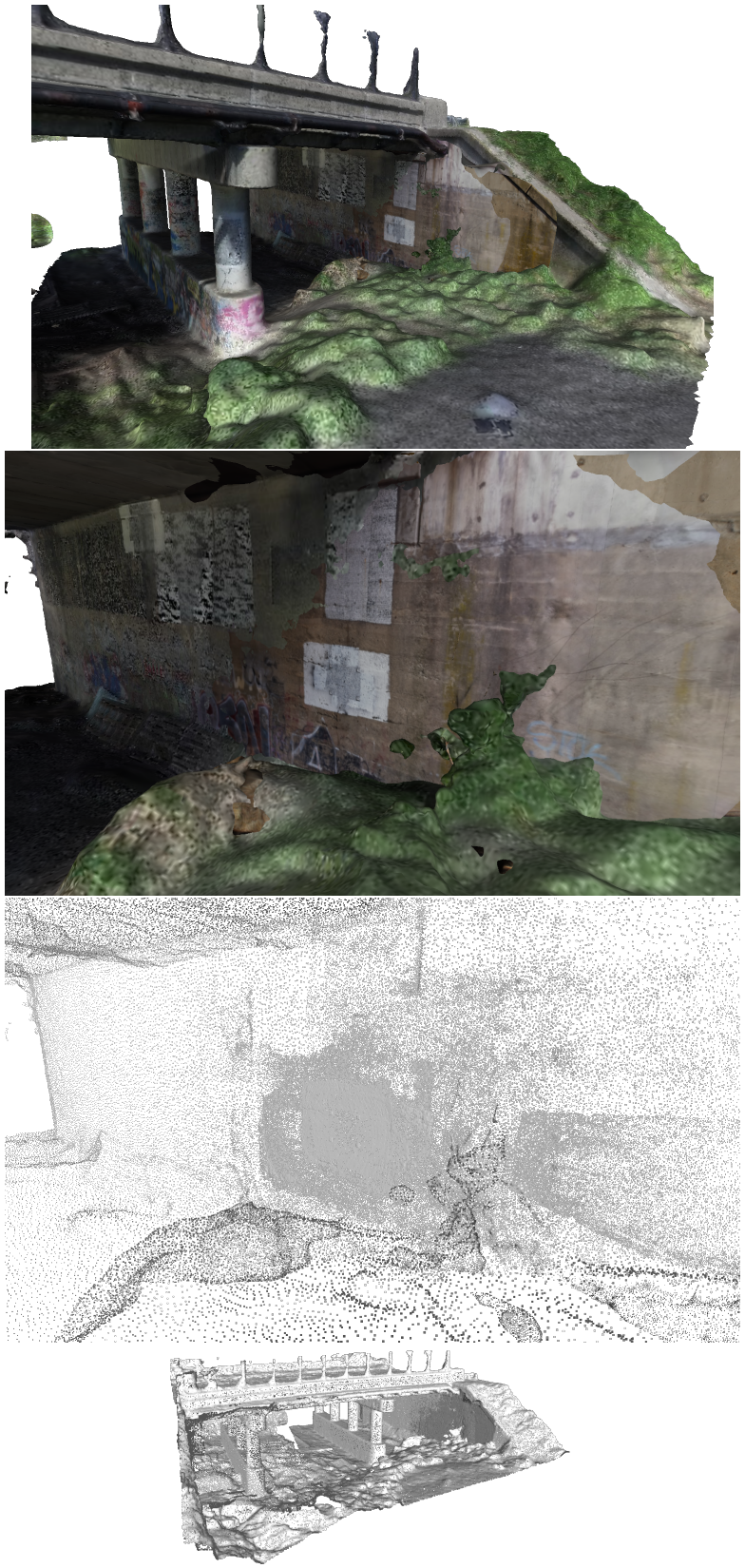

Figure B-1: Plain Street bridge visual inspection model

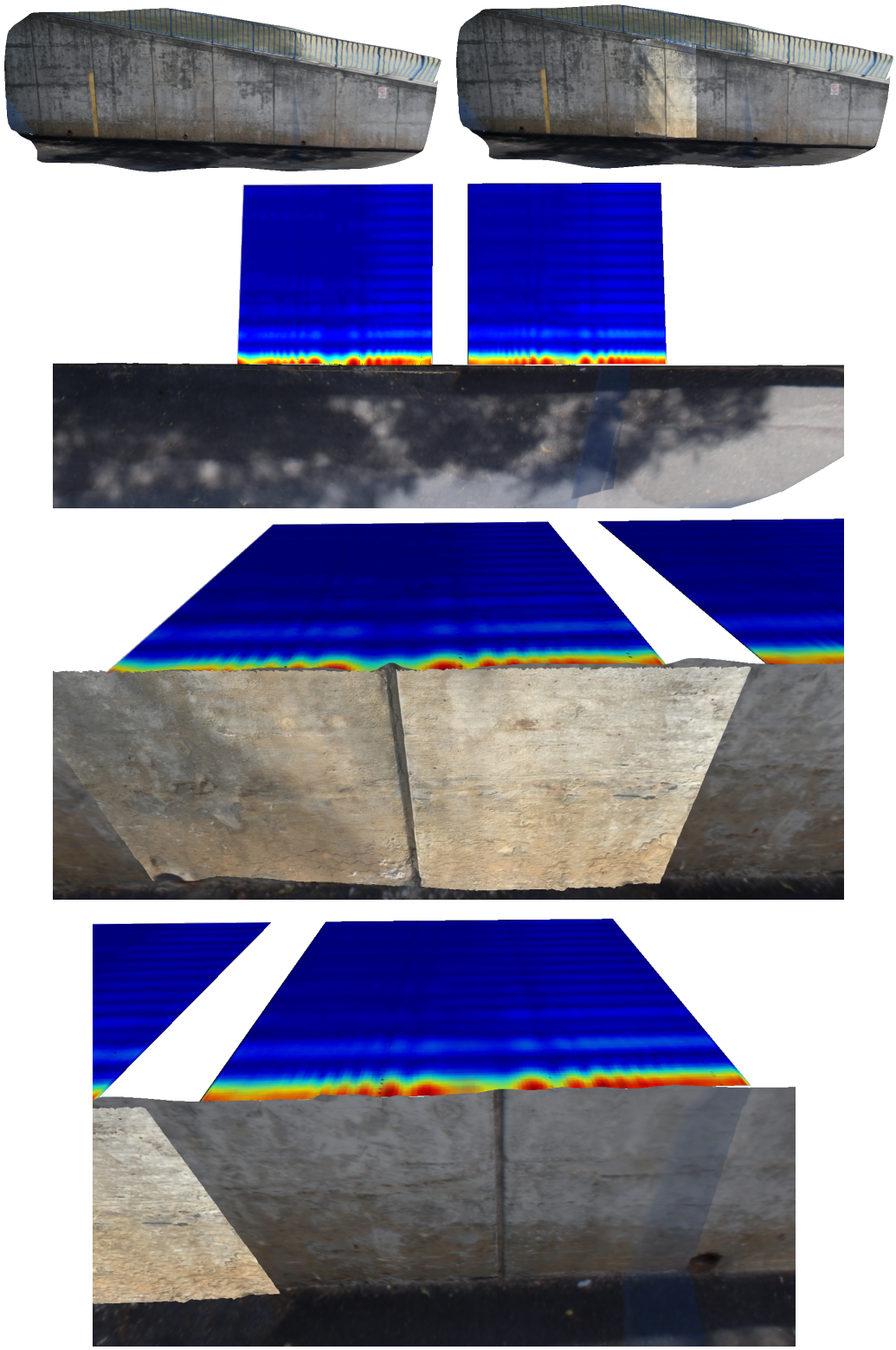

Figure B-2: SAR integration at UMass Lowell's receiving dock

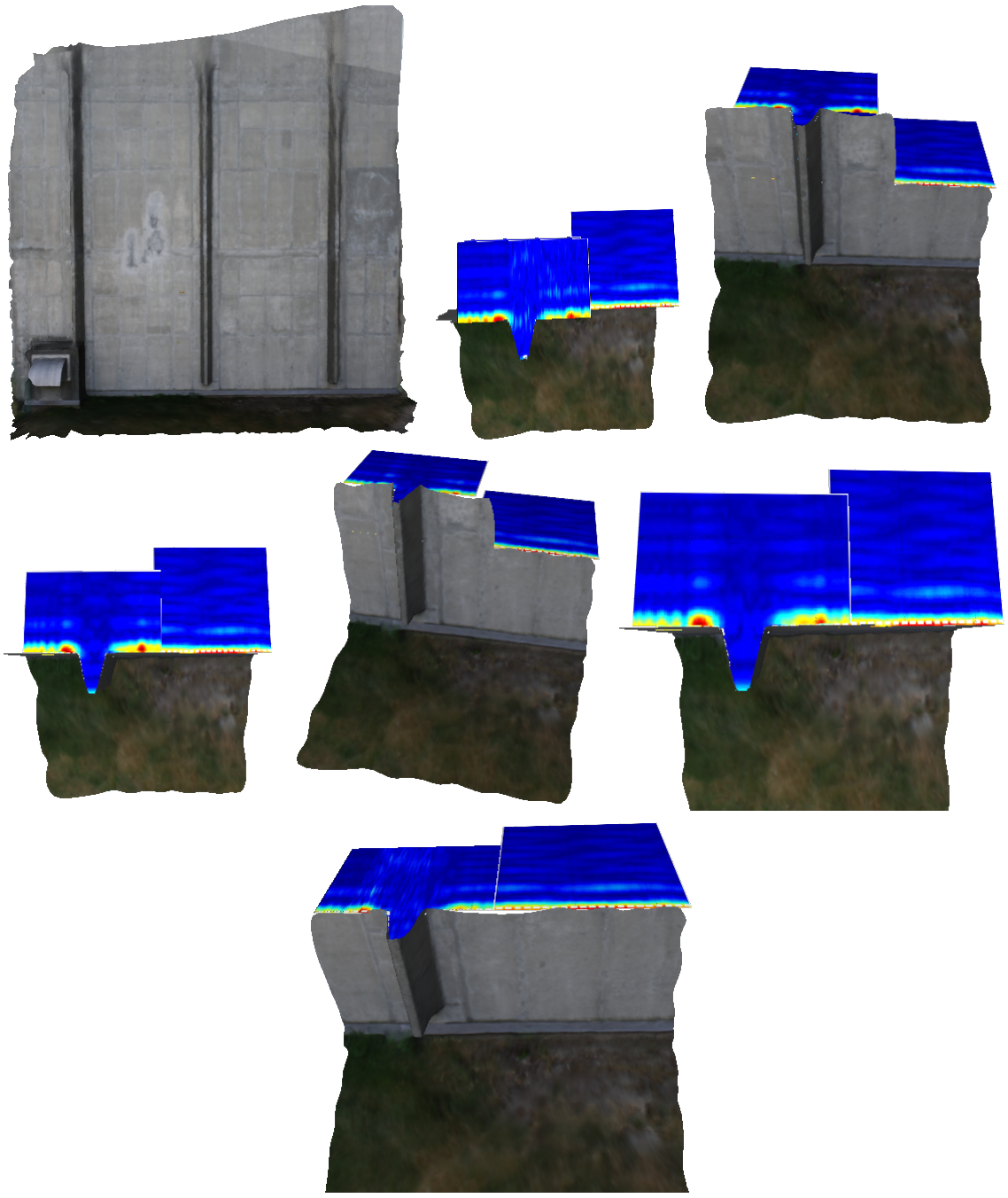

Figure B-3: SAR integration at UMass Lowell's Pinanski Hall

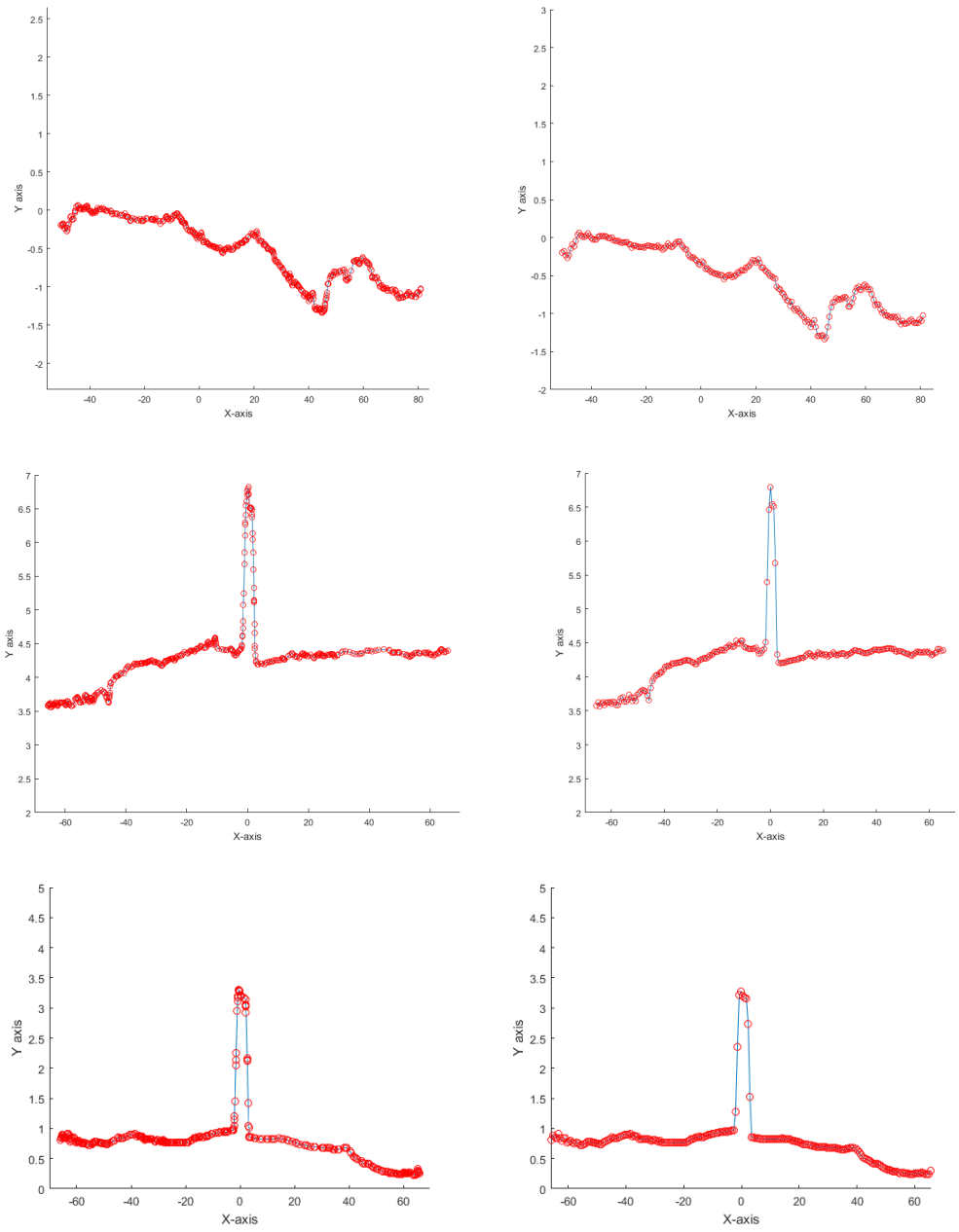

Figure B-4: Motion correction process on SAR images using Photogrammetry

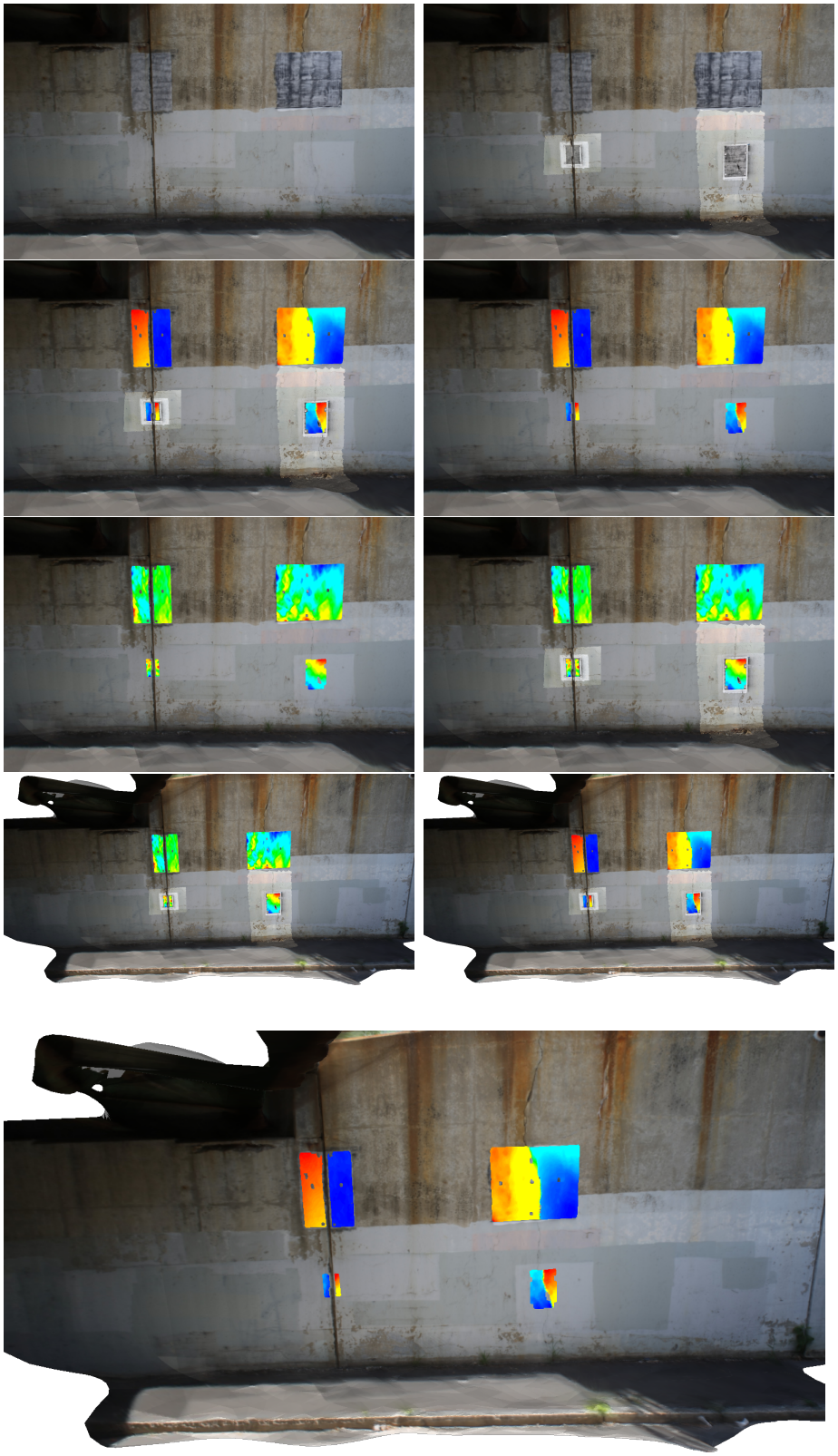

Figure B-5: DIC integration at Lincoln Street bridge, Lowell MA.

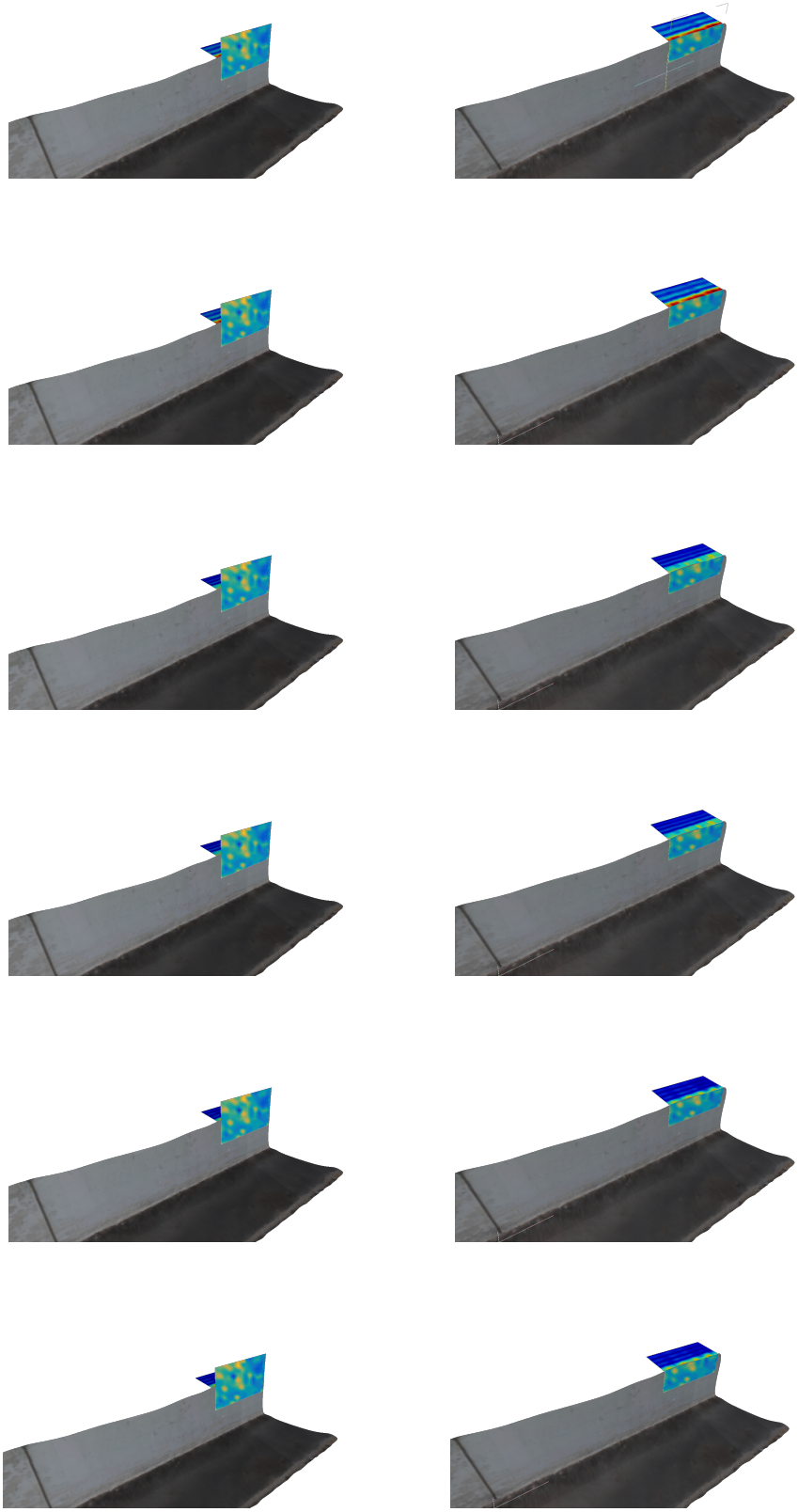

Figure B-6: RBH/SAR integration at Lincoln Street bridge, Lowell MA.

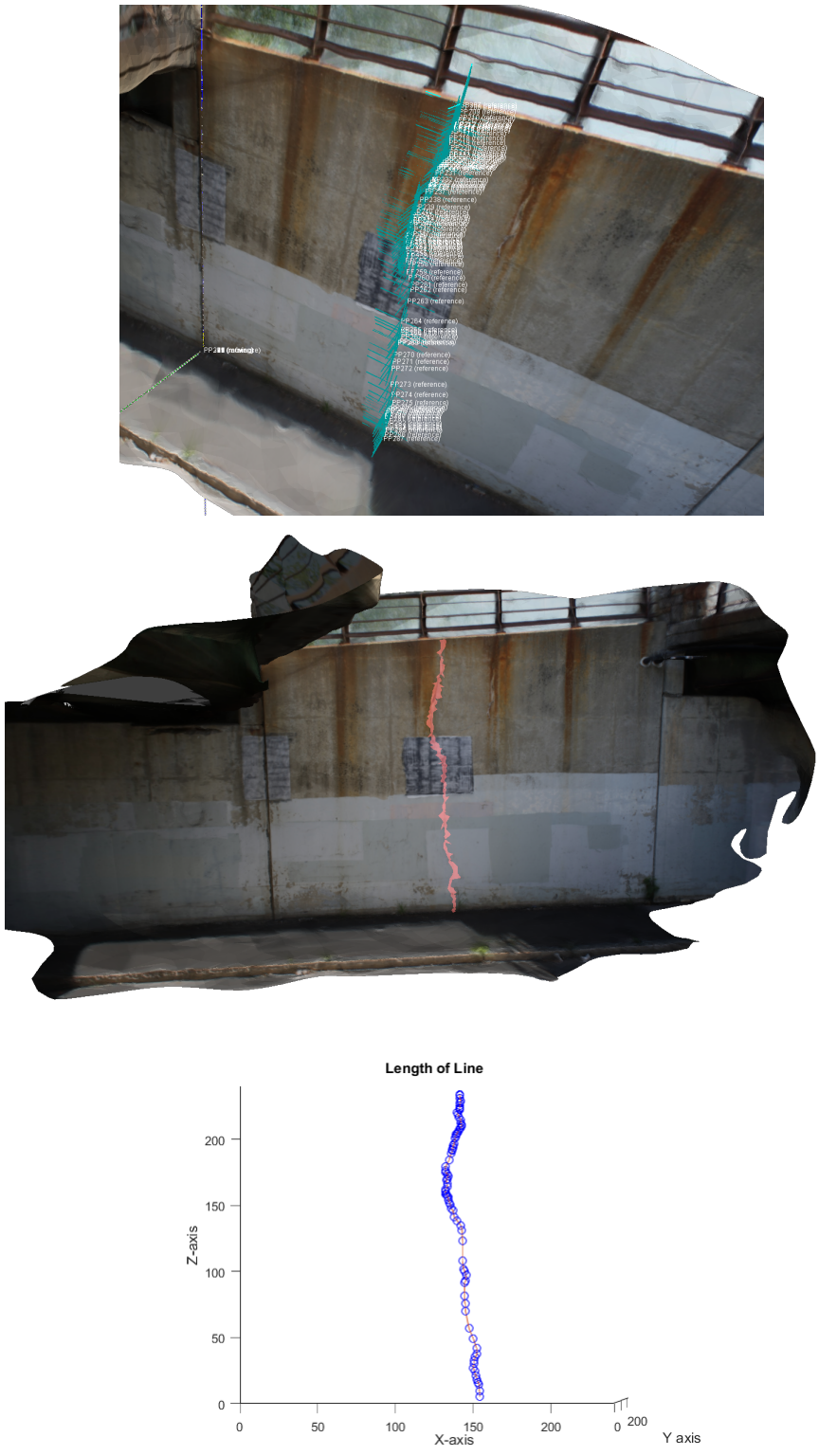

Figure B-7: Surface crack profiling at Lincoln Street bridge, Lowell MA.

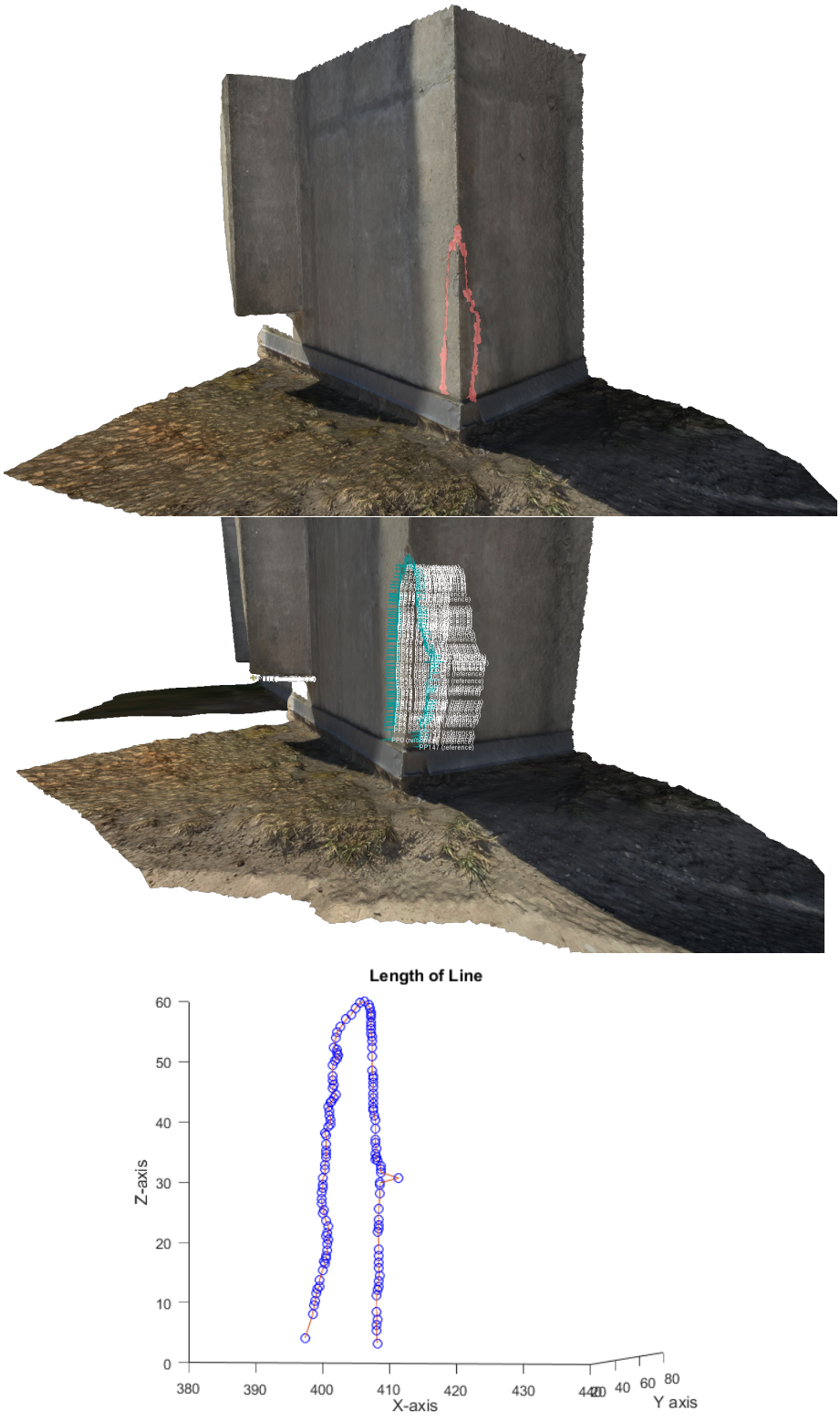

Figure B-8: Surface crack profiling at Pinanski Hall

Appendix C

User Manual

Photogrammetric Tools for Civil Engineers

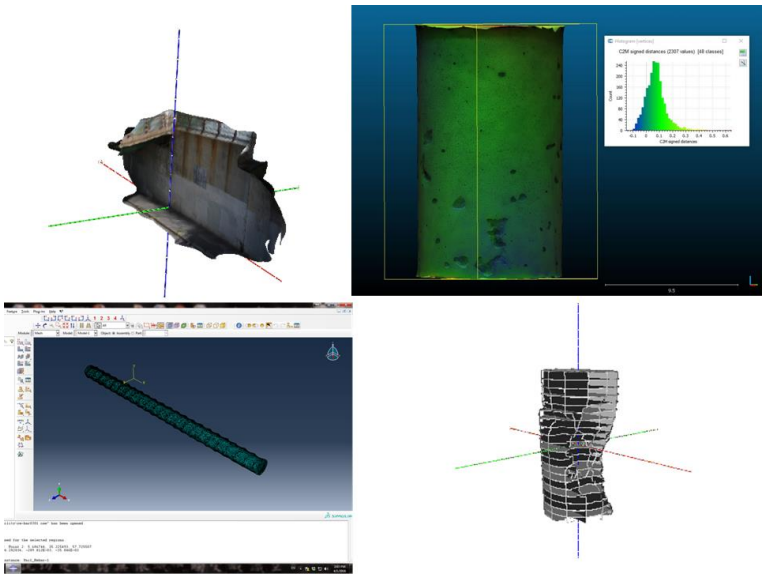

User's Manual

Version 1.0

Table of Contents

Preface

This document contains the procedure for acquiring, and processing photogrammetric surface geometry, surface and material properties data for the condition assessment of concrete structures. This Photogrammetric toolbox cooperatively operates with terrestrial and airborne unmanned aircraft vehicle (UAV) platform. Agisoft's photoscan©. Meshlab, and cloud-compare software's are used for construction and analysis. The airborne platform used is a DJI Phantom 3 professional, and terrestrial platform imagers include phones and cannon (model).

The photogrammetric approach allows for the geometrically accurate construction of buildings, structures and specimens of interest for civil engineers. These models when constructed effectively can be used to determine not only the locations but severities of damages. They may be used for data registration for other data collected in the field and they can may even be used for the mechanical finite element analysis of structures.

Limitations in this approach are the isolated collected of only surface information. Additionally the errors associated with this approach can be linked to several factors which are fairly difficult to control including motion blur, lighting issues, overlapping information and many others. For these reasons the approach requires a level of skill that can only really be adapted with experience.

Necessary Software Packages: Meshlab, Cloud compare, Agisoft Photoscan, Auto-Flight Logic's Autopilot App for Ipad.

Step 1. Data Acquisition

Preparation: Split into Zones (Autopilot, Manual UAV, and Terrestrial)

i. Inspect the subject of interest from all accessible points of view. Take this time to look for any noticeable defects, markings, or areas of high concern.
ii. Place the fiducial marker and scale in areas of low surface texture contrast.

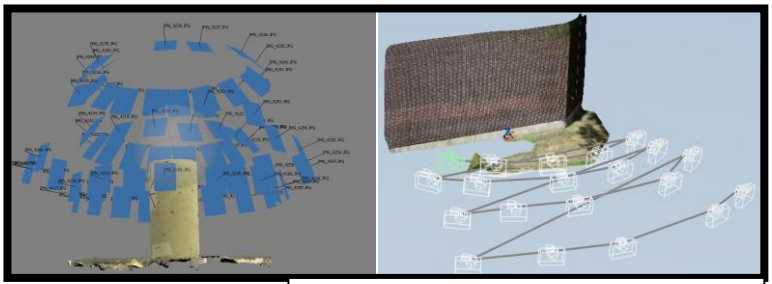

Figure 1: Data acquisition

b. Terrestrial (on foot)

i. Take pictures in a circular formation around the subject of interest.
    1. **Note:** for lab specimen use terrestrial only and collect the data using at least 3 different circles around the subject with variant height/angle/distance combinations

ii. **For internal piers and columns**: treat as separate subjects. Collect the data for these as you would in part (i).

iii. **For walls and abutments:** collect data using at least 2 distances in a semicircle fashion around the wall.

iv. Return to any areas of high concern to get more detailed photographs.

c. Airborne (UAV)

i. Collect airborne videos using at least two flight radii with respectively different angles of perspective. (correlating a larger radius with a smaller angle but maintaining between 55^{o}-35^{o})

ii. For entire structures:

1. Autoilot

a. Manually center the drone above the POI (Ex: the top of the smokestack)
b. Choose radius, speed and altitude and engage autopilot (Save flight plan)
c. Lower altitude until the UAV reaches the manual zone and return home
d. Change battery and repeat with different parameters.
e. Plan out zones by calculating rev/10min battery life

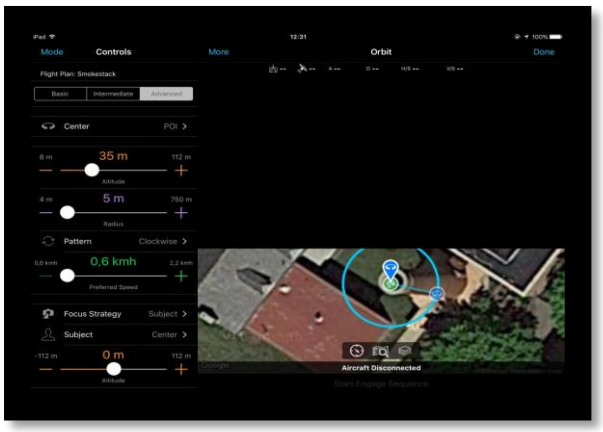

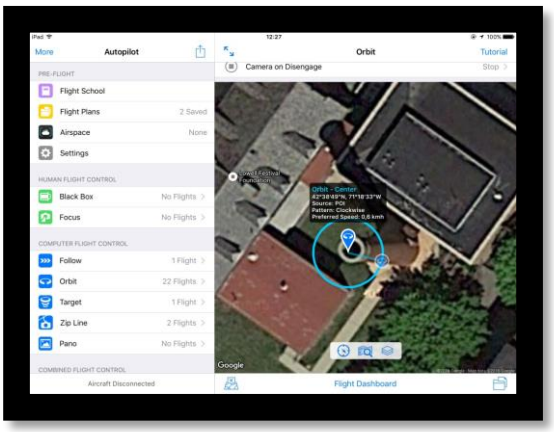

2. **Manual**
    a. Within the Manual Zone the autopilot functionality will not be used to ensure the safety of all personnel involved in inspection. Due to the roof and other obstacles as much area as can be effectively inspected will be carefully recorded

iii. **For internal piers and columns**: treat as separate subjects. Collect the data for these as you would in part (i).
iv. **For walls and abutments:** collect data using at least 2 distances/ height and angle combinations; in a semicircle fashion around the wall.
v. Return to any areas of high concern to get more detailed photographs.

Step 2. Data Processing

a. Extracting images from videos

i. In order to effectively capture the photographs from the 4k resolution video stream used in the acquisition process VLC media player is used in conjunction with its scene extraction filter. To activate the filter go to Tools>Preferences>check advanced>Video>filters>scene
ii. Choose a directory, frame capture rate, and format for image extraction

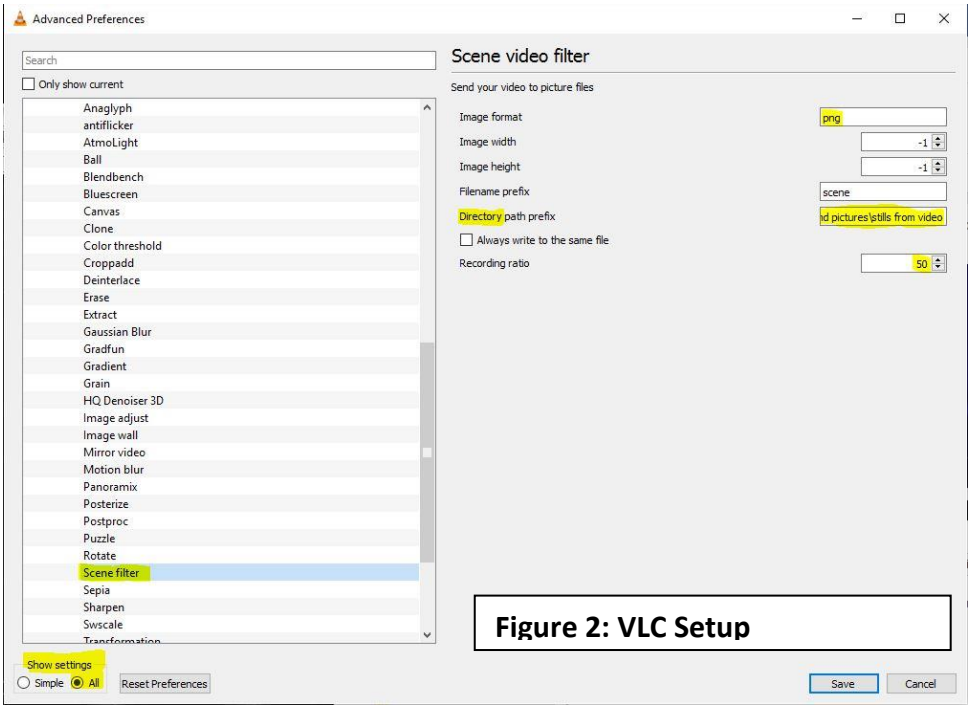

Figure 2: VLC Setup

b. **Data Filtering:** Filter out/ delete any "bad" blurry or unnecessary photos.
c. **Batch Processing:**Batch Process using Agisofts photoscanning software
    i. Align photos
    ii. Build Dense Cloud
    iii. Build Mesh
    iv. Build Texture
d. **Exporting Model:** Export model as .obj and send to Meshlab.

VERY IMPORTANT: at this point the reliability of the processed model needs to be verified using a PCD threshold value of at least 15pt/cm3 If the threshold is not satisfied more data will need to be collected or poor data (photographs) will need to be removed.

Step 3. Data Analysis (In Meshlab and Cloud Compare)

a. **Calibrate the model:** Calibrate the model to the correct size using the calibration fiducial or if not available use the smallest known dimension in an area of highest point cloud density (Meshlab)

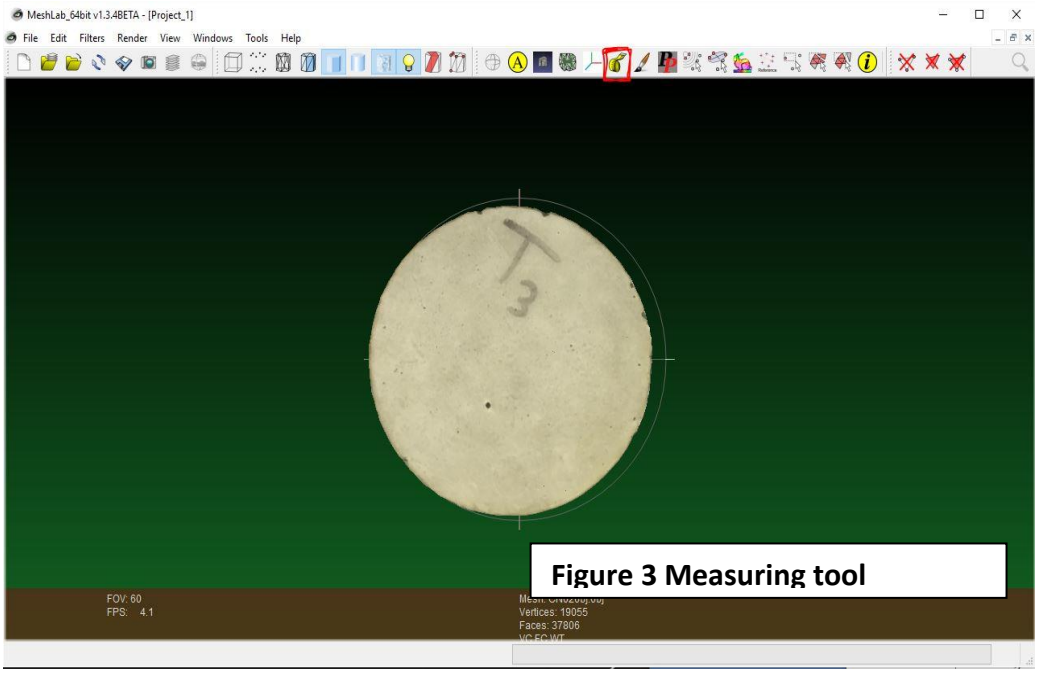

Figure 3 Measuring tool

Use the measuring tape to get the distance and use fliters> Normals,Curvatures, orientation> Transform: scale to adjust the model to it's appropriate scale

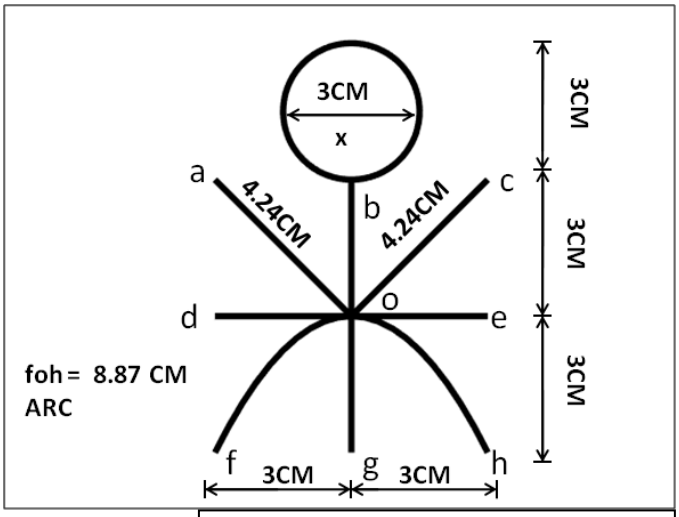

Figure 4: Calibration tool

b. **Clean the Mesh:** Using the selection and delete tools, clean the mesh getting rid of all unnecessary additional information.

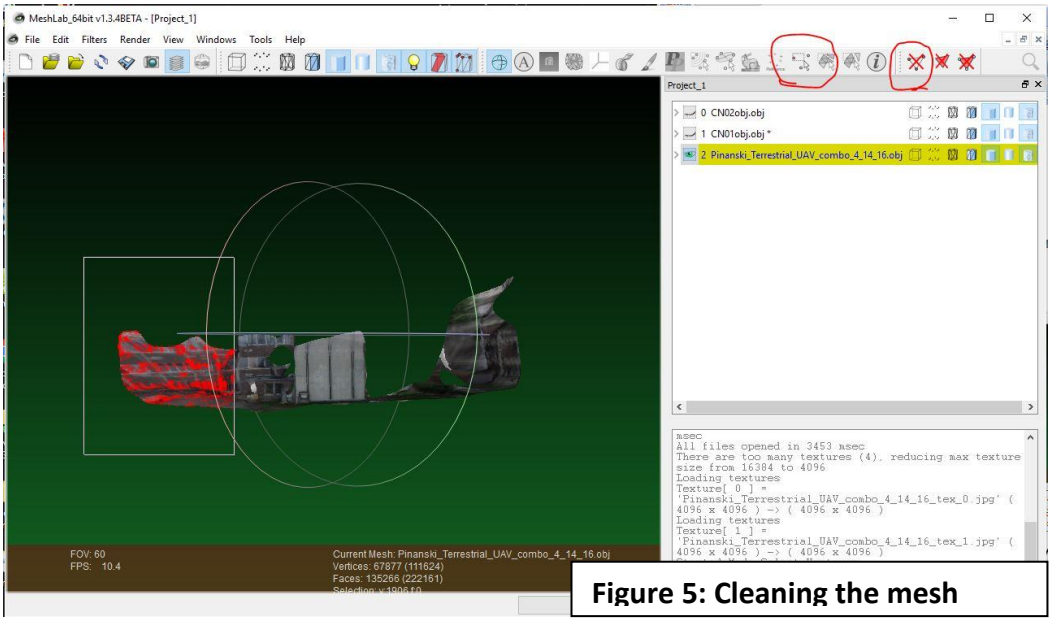

Figure 5: Cleaning the mesh

After cleaning the mesh, the model is ready to be used for any of the established applications which are all done differently. The following will be outlined in this manual

- **Surface Crack Profiling**
- **Surface Profiling**
- **Cross Sectional Analysis**
- **Data registration of SAR rebound hammer and DIC information**
- **Iterative Closest Point analysis**
- **Preparation for Finite element analysis**

c. **Surface Crack Profiling:** using the reference tool add enough points to calculate the overall length. When adding points consider the trajectory of the crack. I.E. curvier sections require more points than along a straight path.

   i. Open the exported reference points and paste them into the excel sheet used in the Matlab code found in the directory described below

Matlab>Photogrammetric Evaluation Techniques>location_size_area

This Matlab code can be used in conjunction with a given set of points to extract the cracks

ii. Use the measuring tool to manually measure and record the widths of the cracks or using reference points as above calculate the disparities.

d. Surface Profiling: For non-closed mesh. The Computation of planar sections can be used to determine a profile of the structures face.

i. Render> Show Axis to turn the x,y,z axis's on.
ii. Use the "manipulator tool to translate and rotate the pint cloud model into a reasonable place to be used for cross sectional analysis. (must be done with respect to an axis so alignment is key here)
iii. Show layer dialogue and right click mesh> freeze current matrix This step ensures that PCM is in place in terms of data and not just visually
iv. Filters> quality measure and computations> compute planar sections
v. Choose plane perpendicular to and adjust the offset to calculate multiple sections (offset represents the location at which the profile will be taken)
vi. Export this profile line as .xyz and open in an excel file. Given multiple profiles, this information could be used to interpret the amount of spalled concrete in different areas of an abutment to calculate damage without having a closed structure.
vii. If the surface profile is to be used to correlate with SAR images use the matlab code below to interpolate data to a given SAR x-range.

Matlab>Photogrammetric Evaluation Techniques>Surface profile code and data> Surface_profile_correction

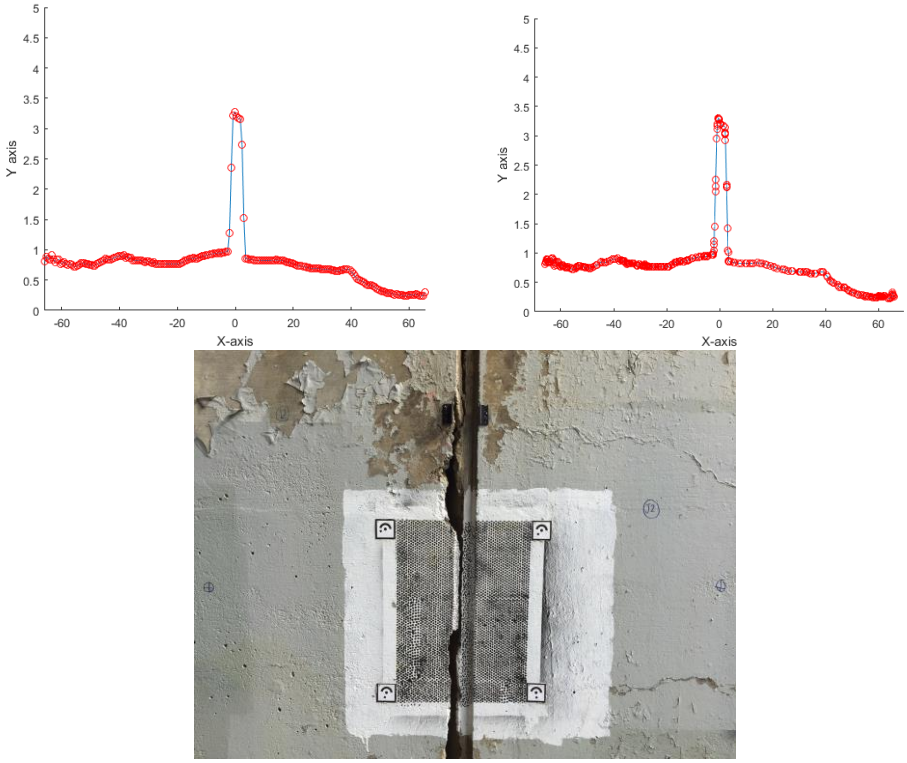

e. **Cross Sectional Analysis:** By computing planar sections, a cross sectional analysis can be performed on concrete specimen and structural components

   i. Render> Show Axis to turn the x,y,z axis's on.
   ii. Use the "manipulator tool to translate and rotate the pint cloud model into a reasonable place to be used for cross sectional analysis. (must be done with respect to an axis so alignment is key here)
   iii. Show layer dialogue and right click mesh> freeze current matrix This step ensures that PCM is in place in terms of data and not just visually
   iv. Filters> quality measure and computations> compute planar sections
   v. Choose plane perpendicular to and adjust the offset to calculate multiple sections **(Make sure create also section surface is checked and before each section is computed reselect the PCM of interest as it will deselect automatically)**

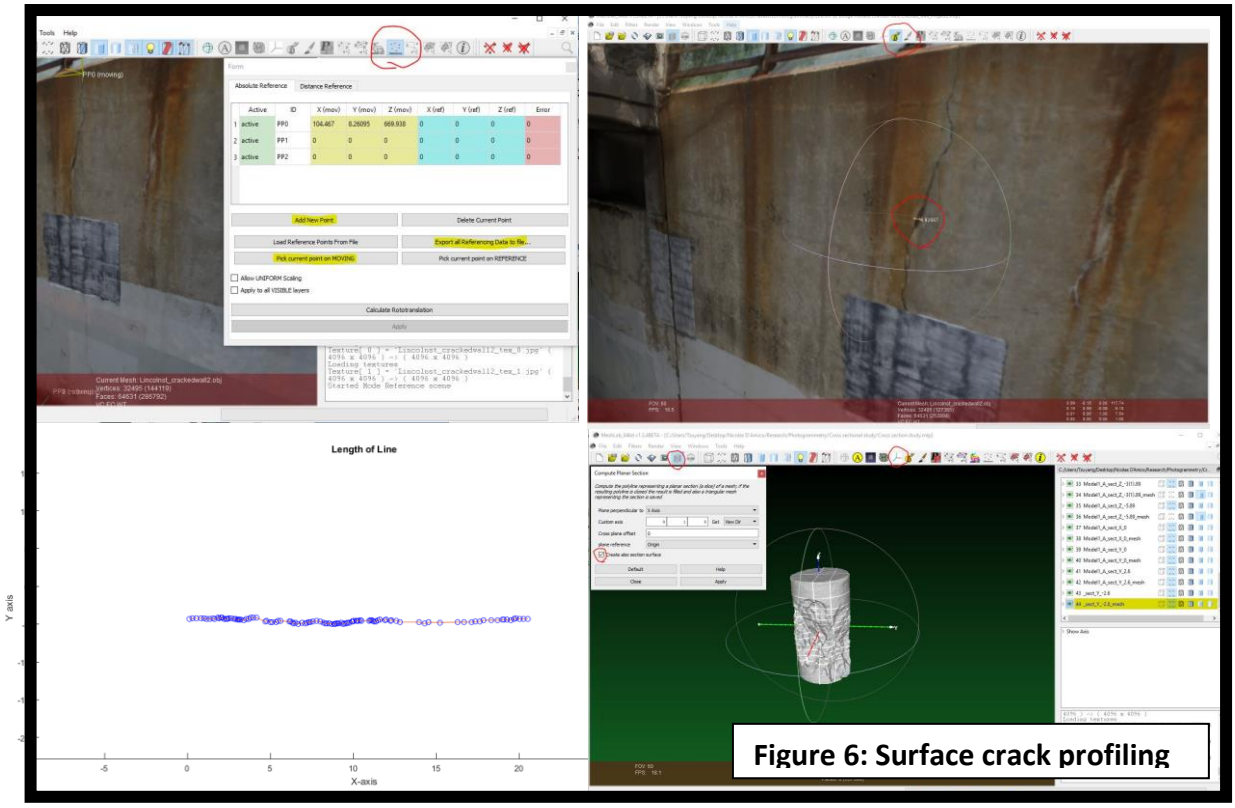

Figure 6: Surface crack profiling

f. Data Registration: for SAR, DIC, rebound Hammer etc.

i. If **.stl** available disregard steps below, and manually align
ii. Filters> Create new mesh layer>Fractal terrain (set max height to zero to create a flat uniform plane)
iii. Import the Jpeg files which are to be registered into the point cloud model these will be shown in the raster section of the layer dialogue.
iv. Select the Show current Raster mode select the raster of choice and position the flat mesh plane into place
v. Filters>Camera>project active raster color to current mesh.
vi. Cut and scale to appropriate size.
vii. Using the manipulator tool place the data in the appropriate location

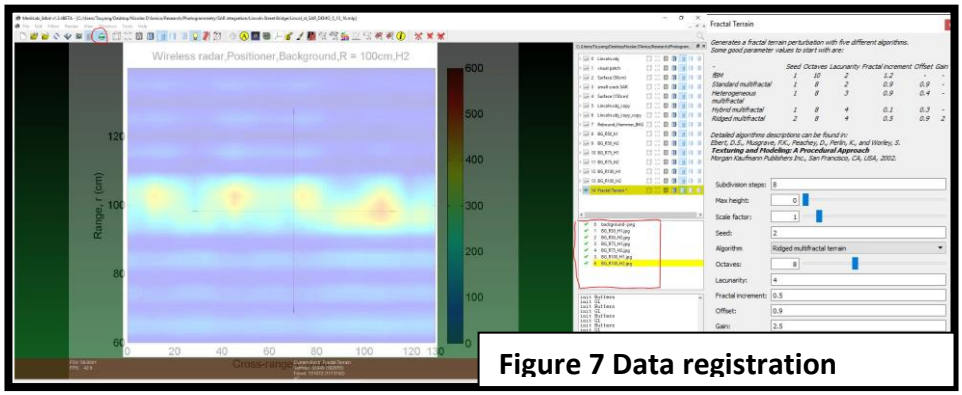

Figure 7 Data registration

g. Iterative Closest Point Analysis

i. Export or save models of interest as .obj files. At least 2 similar models are needed for this type of evaluation

ii. Import the files into cloud compare

iii. Use the rough alignment tool (not allowing for scaling) to automatically align the models.

iv. Select 2 models and using the compute cloud/mesh distance calculate the iterative disparities in the closest points. This will visually show the change in distance between 2 respective closest points between models. This information may be used to correlate to loading, strain, and deflection of specimen and structures

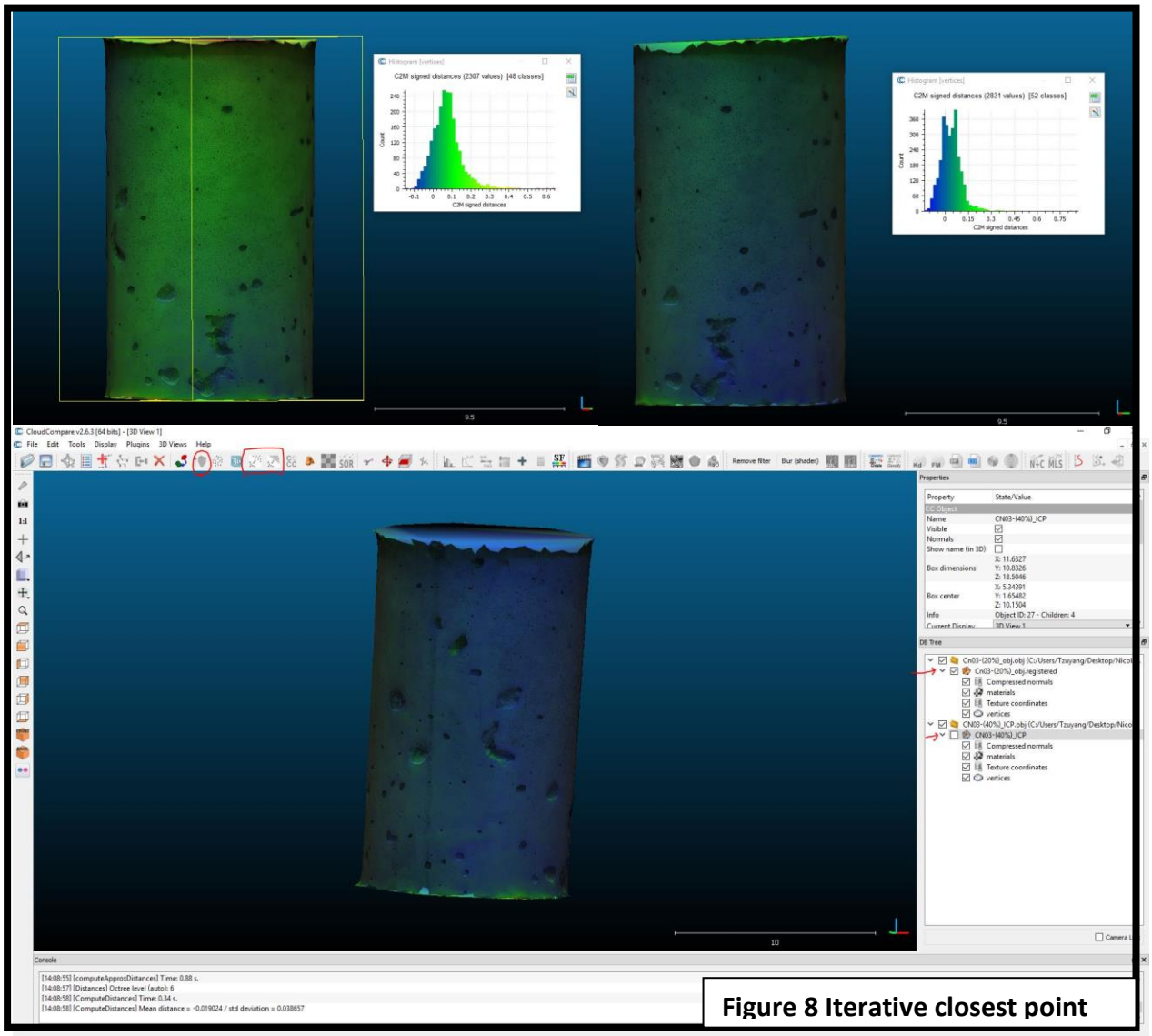

Figure 8 Iterative closest point

h. **Preparation for finite element analysis:** preparation for Finite element analysis requires a uniform mesh grid, and a conversion from .stl (shell) to .sat (which is a solid object)
    i. Import model of interest as .obj into Meshlab
    ii. Filters>Remeshing, Simplification, and reconstruction> Surface reconstruction:VCG –or- **Sim plify mesh**
    iii. Export as a .stl file into matlab folder shown below

iv. Matlab>Rebar Modeling>Rebar Conversion> type in the file of choice

v. .sat output is ready for FEA

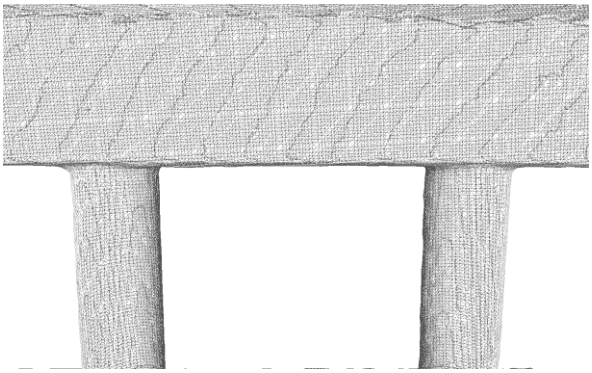

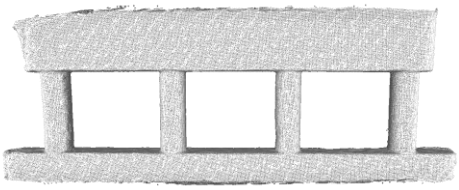

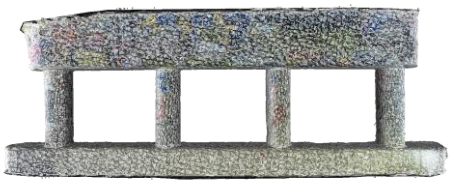

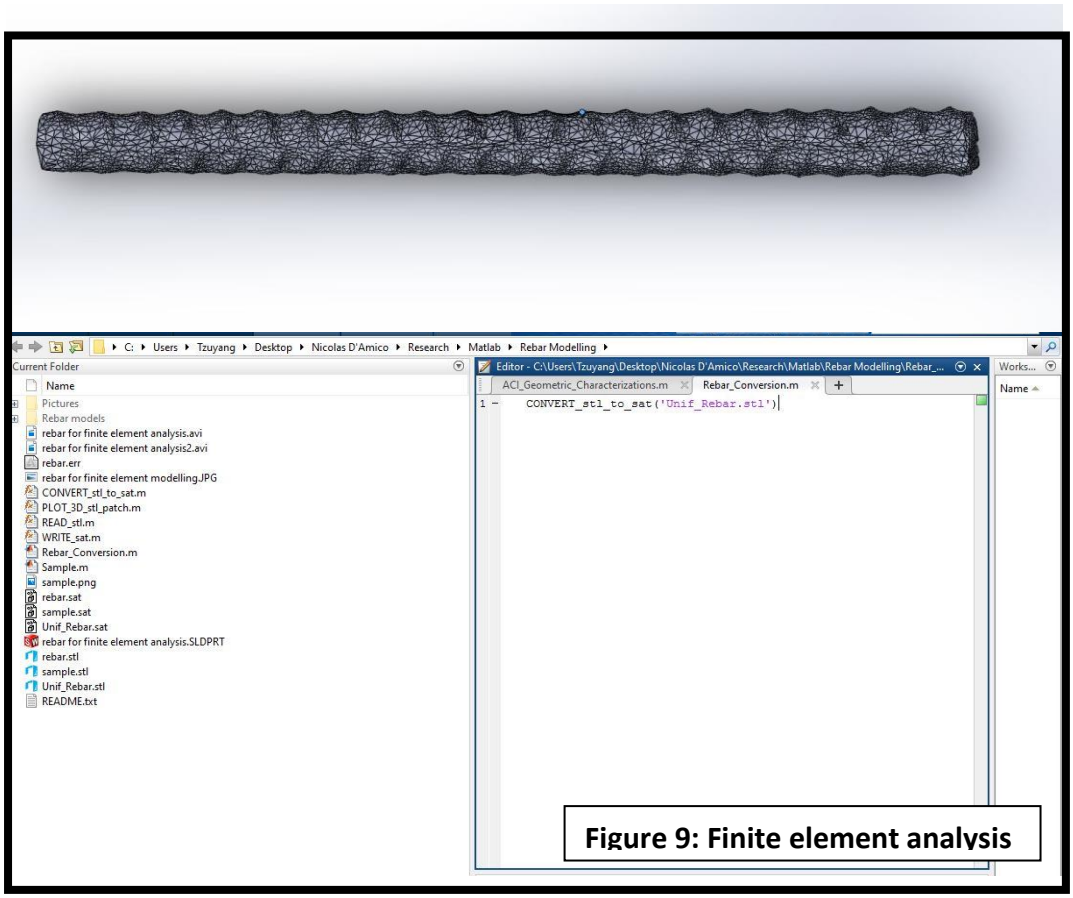

Figure 9: Finite element analysis

Bibliography

[1] G. Almeida, H. Biscaia, C. Chastre, J. Fonseca, and F. Melcio. Displacement estimation of a rc beam test based on tss algorithm. In *Information Systems and Technologies (CISTI), 2010 5th Iberian Conference on*, pages 1–4, June 2010.

[2] Pedro Arias, J. Carlos Caama n o, Henrique Lorenzo, and Julia Armesto. 3d modeling and section properties of ancient irregular timber structures by means of digital photogrammetry. *Computer-Aided Civil and Infrastructure Engineering*, 22(8):597–611, nov 2007.

[3] J. Bdkowski, M. Peka, K. Majek, T. Fitri, and J. Naruniec. Open source robotic 3d mapping framework with ros x2014; robot operating system, pcl x2014; point cloud library and cloud compare. In *Electrical Engineering and Informatics (ICEEI), 2015 International Conference on*, pages 644–649, Aug 2015.

[4] Sean P. Bemis, Steven Micklethwaite, Darren Turner, Mike R. James, Sinan Akciz, Sam T. Thiele, and Hasnain Ali Bangash. Ground-based and uav-based photogrammetry: A multi-scale, high-resolution mapping tool for structural geology and paleoseismology. *Journal of Structural Geology*, 69, Part A:163 – 178, 2014.

[5] Edward M. Mikhail James S. Bethel and J.Chris McGlone. *Introduction to Modern Photogrammetry*. John Wiley and Sons Inc., 605 Third Avenue New York NY, 2001.

[6] Thomass Luhmann Stuart Robson Stephen Kyle Jan Boehn. *Close-Range Photogrammetry and 3D Imaging*. Walter de Gruter Gmbh and Co. KG; Gottingen., 121 High St. Boston, MA, 2nd edition, 2014.

[7] Krisada Chaiyasarn, Tae-Kyun Kim, Fabio Viola, Roberto Cipolla, and Kenichi Soga. Distortion-free image mosaicing for tunnel inspection based on robust cylindrical surface estimation through structure from motion. *Journal of Computing in Civil Engineering*, 0(0):04015045, 2015.

[8] Paolo Cignoni, Marco Callieri, Massimiliano Corsini, Matteo Dellepiane, Fabio Ganovelli, and Guido Ranzuglia. Meshlab: an open-source mesh processing tool. In Vittorio Scarano, Rosario De Chiara, and Ugo Erra, editors, *Eurographics Italian Chapter Conference*. The Eurographics Association, 2008.

[9] I. Colomina and P. Molina. Unmanned aerial systems for photogrammetry and remote sensing: A review. *Journal of Photogrammetry and Remote Sensing*, 92:79 – 97, 2014.

[10] Nicolas DAmico and Tzuyang Yu. Photogrammetric analysis of concrete specimens and structures for condition assessment. In Tzuyang Yu, Andrew L. Gyekenyesi, Peter J. Shull, and H. Felix Wu, editors, *Nondestructive Characterization and Monitoring of Advanced Materials, Aerospace, and Civil Infrastructure 2016*. SPIE-Intl Soc Optical Eng, apr 2016.

[11] Nicolas DAmico and Tzuyang Yu. Accuracy analysis of point cloud modeling for evaluating concrete specimens. In H. Felix Wu, Andrew L. Gyekenyesi, Peter J. Shull, and Tzu-Yang Yu, editors, *Nondestructive Characterization and Monitoring of Advanced Materials, Aerospace, and Civil Infrastructure 2017*. SPIE, apr 2017.

[12] David Lattanzi and Gregory Miller. 3d scene reconstruction for robotic bridge inspection. *Journal of Infrastructure Systems*, 21(2):04014041, 2015.

[13] Habib Fathi and Ioannis Brilakis. Automated sparse 3d point cloud generation of infrastructure using its distinctive visual features. *Advanced Engineering Informatics*, 25(4):760 – 770, 2011. Special Section: Advances and Challenges in Computing in Civil and Building Engineering.

[14] Matthew N. Gillins, Daniel T. Gillins, and Christopher Parrish. Cost-effective bridge safety inspections using unmanned aircraft systems (uas). In *Geotechnical and Structural Engineering Congress 2016*. American Society of Civil Engineers (ASCE), feb 2016.

[15] A. Ardeshir Goshtasby. *2-D AND 3-D Image Registration for medical, remote sensing and industrial applications*. John Wiley and Sons Inc., 111 River Street Hoboken, NJ, 2001.

[16] Bahman Jafari, Ali Khaloo, and David Lattanzi. Long-term monitoring of structures through point cloud analysis. volume 9805, pages 98052K–98052K–8, 2016.

[17] M.R. James, S. Robson, S. d'Oleire Oltmanns, and U. Niethammer. Optimising uav topographic surveys processed with structure-from-motion: Ground control quality, quantity and bundle adjustment. *Geomorphology*, pages –, 2016.

[18] I. Kalisperakis, C. Stentoumis, L. Grammatikopoulos, M.E. Dasiou, and I.N. Psycharis. Precise 3d recording for finite element analysis. In *2015 Digital Heritage*. Institute of Electrical and Electronics Engineers (IEEE), sep 2015.

[19] R. A. Kuccak, F. Kilic, and A. Kisa. Analysis of terrestrial laser scanning and photogrammetry data for documentation of historical artifacts. *ISPRS - International Archives of the Photogrammetry, Remote Sensing and Spatial Information Sciences*, XLII-2/W1:155–158, oct 2016.

[20] Hans-Gerd Maas and Uwe Hampel. Photogrammetric techniques in civil engineering material testing and structure monitoring. *ISPRS Journal of Photogrammetric Engineering and Remote Sensing*, 2006.

[21] C. MacNish, G. M. Hassan, A. V. Dyskin, and E. Pasternak. Towards affordable and robust remote photogrammetric sensing for early warning of fracturing and structural failure. In *Humanitarian Technology Conference (R10-HTC), 2015 IEEE Region 10*, pages 1–6, Dec 2015.

[22] R. El Meouche, I. Hijazi, P. A. Poncet, M. Abunemeh, and M. Rezoug. Uav photogrammetry implementation to enhance land surveying, comparisons and possibilities. *ISPRS - International Archives of the Photogrammetry, Remote Sensing and Spatial Information Sciences*, XLII-2/W2:107–114, oct 2016.

[23] Dong Mingli, Wang Jun, Yan Bixi, Lou Xiaoping, and Chen Ruibao. Accuracy evaluation method and experiments for photogrammetry based on 3d reference field. In *Advanced Technology of Design and Manufacture (ATDM 2010), International Conference on*, pages 489–492, Nov 2010.

[24] Logan M. Palmer, Kevin W. Franke, R. Abraham Martin, Brendan E. Sines, Kyle M. Rollins, and John D. Hedengren. *Application and Accuracy of Structure from Motion Computer Vision Models with Full-Scale Geotechnical Field Tests*, pages 2432–2441.

[25] J. Reznicek, T. Luhmann, and C. Jepping. Influence of raw image preprocessing and other selected processes on accuracy of close-range photogrammetric systems according to vdi 2634. *Int. Arch. Photogramm. Remote Sens. Spatial Inf. Sci.*, XLIB5:107–113, jun 2016.

[26] Radu Bogdan Rusu, Zoltan Csaba Marton, Nico Blodow, Mihai Dolha, and Michael Beetz. Towards 3d point cloud based object maps for household environments. *Robotics and Autonomous Systems*, 56(11):927 – 941, 2008. Semantic Knowledge in Robotics.

[27] S Sankarasrinivasan, E Balasubramanian, K Karthik, U Chandrasekar, and Rishi Gupta. Health monitoring of civil structures with integrated uav and image processing system. *Procedia Computer Science*, 54:508–515, 2015.

[28] P. Sapirstein. Accurate measurement with photogrammetry at large sites. *Journal of Archaeological Science*, 66:137 – 145, 2016.

[29] Q. Shi and N. Xi. Automated data processing for a rapid 3d surface inspection system. In *Robotics and Automation, 2008. ICRA 2008. IEEE International Conference on*, pages 3939–3944, May 2008.

[30] Kenichi Soga. *Innovation in Instrumentation, Monitoring, and Condition Assessment of Infrastructure*, pages 465–489. Springer International Publishing, Cham, 2016.

[31] M. Solla, J.C. Caamao, B. Riveiro, and P. Arias. A novel methodology for the structural assessment of stone arches based on geometric data by integration of photogrammetry and ground-penetrating radar. *Engineering Structures*, 35:296 – 306, 2012.

[32] M.E. Stavroulaki, B. Riveiro, G.A. Drosopoulos, M. Solla, P. Koutsianitis, and G.E. Stavroulakis. Modelling and strength evaluation of masonry bridges using terrestrial photogrammetry and finite elements. *Advances in Engineering Software*, pages –, 2016.

[33] Simon Stent, Riccardo Gherardi, Bjorn Stenger, Kenichi Soga, and Roberto Cipolla. Visual change detection on tunnel linings. *Machine Vision and Applications*, 27(3):319–330, nov 2014.

[34] Scott Swearingen and Kyoung Lee Swearingen. Creating virtual environments with 3d printing and photogrammetry. In *SIGGRAPH ASIA 2016 Creating Virtual Environments on*. Association for Computing Machinery (ACM), 2016.

[35] Athanasios Voulodimos Nikolaos Doulamis Dieter Fritsch Konstantinos Makantasis Anastasios Doulamis and Michael Klein. Four-dimensional reconstruction of cultural heritage sites based on photogrammetry and clustering. *Journal of Electronic Imaging*, 26(1):011013, 2016.

[36] Sara B. Walsh, Daniel J. Borello, Burcu Guldur, and Jerome F. Hajjar. Data processing of point clouds for object detection for structural engineering applications. *Computer-Aided Civil and Infrastructure Engineering*, 28(7):495–508, may 2013.

[37] JJ Wang, N Gowripalan, J Li, and VV Nguyen. Close-range photogrammetry for accurate deformation distribution measurement. In *Mechanics of Structures and Materials: Advancements and Challenges*, pages 793–800. CRC Press, 2016.

[38] M.J. Westoby, J. Brasington, N.F. Glasser, M.J. Hambrey, and J.M. Reynolds. structure-from-motion photogrammetry: A low-cost, effective tool for geoscience applications. *Geomorphology*, 179:300 – 314, 2012.

[39] Yong Zhang, Xiuxiao Yuan, Yi Fang, and Shiyu Chen. Uav low altitude photogrammetry for power line inspection. *Sciprints*, aug 2016.